2010

Interconversion of the Specificities of Human Lysosomal Enzymes

Ivan B. Tomasic
University of Massachusetts Amherst

INTERCONVERSION OF THE SPECIFICITIES OF HUMAN LYSOSOMAL ENZYMES

A Thesis Presented

by

IVAN B. TOMASIC

Submitted to the Graduate School of the
University of Massachusetts Amherst in partial fulfillment
of the requirements for the degree of

MASTER OF SCIENCE

September 2010

Molecular and Cellular Biology

INTERCONVERSION OF THE SPECIFICITIES OF HUMAN LYSOSOMAL ENZYMES

A Thesis Presented

by

IVAN B. TOMASIC

Approved as to style and content by:

Scott C. Garman, Chair

Daniel N. Hebert, Member

Karsten Theis, Member

David Gross, Department Head
Department of Molecular and Cellular Biology

ACKNOWLEDGEMENTS

I would like to thank my advisor Dr. Scott C. Garman for his always extremely helpful guidance and patience, of without which this project would not have been possible. I would also like to thank Dr. Abigail Guce, who mentored me from the first day I arrived in the laboratory and taught me almost everything I know. My collaborator Matt Metcalf was instrumental in this project, and I will always be grateful for his helpful advice and cherish the time we spent working together. Cassidy Dobson also deserved thanks for always providing helpful advice and support, but more importantly she was always a great friend without whom I do not believe this project would have been completed. To my other fellow colleagues and friends, Nat Clark, Jerome Rogich, Yurie Kim, Nilima Kolli, and Yadilette Rivera Colón, you have always been there for me, and I have always valued your advice. I'm sure that all of you will go on to do great things in the times to come, and I thank you all. Finally, I would like to thank my parents, Boris and Marisa Tomasic, for their unwavering support throughout these last two years.

Thank you,

Ivan B. Tomasic

ABSTRACT

INTERCONVERSION OF THE SPECIFICITIES OF HUMAN LYSOSOMAL ENZYMES

SEPTEMBER 2010

IVAN B. TOMASIC, B.S., UNIVERSITY OF MASSACHUSSETS AMHERST

M.S., UNIVERSITY OF MASSACHUSSETS AMHERST

Directed by: Professor Scott C. Garman

Fabry disease (FD) is an X-linked recessive lysosomal storage disorder (LSD) known to affect approximately 1 in every 40,000 males, and a smaller number of females. FD results from a deficiency of functional α-galactosidase (α-GAL), which leads to the accumulation of terminally α-galactosylated substrates in the lysosome. The predominant treatment is Enzyme Replacement Therapy (ERT), requiring the regular infusion of recombinant human α-GAL. More than half of individuals receiving ERT experience a range of adverse infusion reactions, and it has been reported that as many as 88% of patients receiving ERT develop neutralizing IgG antibodies against the drug[7].

In aim of designing a non-immunogenic treatment candidate for Fabry disease ERT, we have engineered the active sites of α-GAL and another homologous family 27 exoglycosylase named α-N-acetylgalactosaminidase (α-NAGAL) to have interconverted substrate specificities. 11 of 13 active site residues are conserved between these two enzymes, and we have shown that their substrate specificities can be interconverted by mutating the two non-conserved active-site residues. We report the kinetic properties of these two mutants along with wild type controls, and use western blotting to show that both mutant enzymes retain their respective wild type enzyme antigenicity. Structural

data obtained by X-ray crystallography on the α-GAL mutant (called α-GAL^{SA}) reveals the mechanism by which substrate specificity is dictated between these two proteins, and provides explanations for the mutant's reduced catalytic efficiency.

TABLE OF CONTENTS

Page

ACKNOWLEDGEMENTS iv

ABSTRACT v

LIST OF TABLE ix

LIST OF FIGURES x

LIST OF SYMBOLS AND ABREVIATIONS xi

CHAPTER

1. INTRODUCTION 1

    1.1 LSDs 1
    1.2 Problems with ERT 2
    1.3 α-N-Acetyl-Galactosaminidase 4
    1.4 Solution to ERT Immune-Response Problems 4

2. RESULTS 7

    2.1 PCR Mutagenesis 7
    2.2 Ligation and Transformation 8
    2.3 DNA Sequencing 8
    2.4 Stable Cell Line 8
    2.5 Large-Scale Expression and Purification 9
    2.6 Ni Affinity Chromatography 1 9
    2.7 Ni Purification 2 10
    2.8 Anion Exchange Chromatography 11
    2.9 Immunogenicity 11
    2.10 pNP Activity Assays 12
    2.11 Optimal pH and Buffer Conditions 12
    2.12 Specific Activity 13
    2.13 Michaelis-Menten Kinetics 13
    2.14 X-ray Crystallography 15

3. DISCUSSION 18

4. SUMMARY 21

5. METHODS 22

5.1 PCR Mutagenesis.....22
5.2 Ligation, Transformation, and Sequencing.....23
5.3 Transfection 23
5.4 Large Scale Expression and Purification of α-GAL^{SA}.....24
5.5 Michaelis Menten Kinetics 25
5.6 Crystallography.....26
5.7 X-Ray Data Collection and Refinement 28

6. FIGURES.....29

APPENDICES

A. PROTOCOLS 50

B. SEQUENCES.....59

C. TOMASIC, I.B., METCALF, M.C., GUCE, A.I., CLARK, N.E., GARMAN, S.C. (MAY 5, 2010) "INTERCONVERSION OF THE SPECIFICITIES OF HUMAN LYSOSOMAL ENZYMES ASSOCIATED WITH FABRY AND SCHINDLER DISEASES." *JBC*, PMID 20444686. 61

BIBLIOGRAPHY.....74

LIST OF TABLE

Table Page

1. α-GAL^{SA} Data Collection and Refinement Statistics 49

LIST OF FIGURES

Figure Page

1. Structure of Human α-GAL and α-NAGAL 29
2. PCR Mutagenesis Gel 30
3. Restriction Digest Gel.....31
4. DNA Sequence Chromatogram of α-GAL^{SA} 32
5. Map of the pIB-V5-His-TOPO-α-GAL (4.85 kb) 33
6. α-GAL^{SA} Stable Cell Line 34
7. Western Blots of α-GAL^{SA} 35
8. Purification Overview.....36
9. Tangential Flow Setup 37
10. Ni Purification # 1.....39
11. Ni Purification # 2.....39
12. Anion Exchange Chromatography Purification.....40
13. α-GAL^{SA} and α-NAGAL^{EL} Biochemistry.....41
14. Optimal pH and Buffer for α-GAL^{SA}.....42
15. α-GAL^{SA} Specific-Activity 43
16. Michaelis-Menten Kinetic Data.....44
17. α-GAL^{SA} Crystals 45
18. α-GAL^{SA} Diffraction Images 46
19. Crystal Structures of α-GAL^{SA} 47

LIST OF SYMBOLS AND ABREVIATIONS

α-GAL ..... α-galactosidase
α-GAL^{SA} ..... α-galactosidase E203S/L206A active site mutant
α-NAGAL ..... α-N-acetylgalactosaminidase
α-NAGAL^{EL} ..... α-N-acetylgalactosaminidase S188E/A191L active site mutant
α-Gal ..... α-galactose
α-GalNAc ..... α-N-acetylgalactosamine
ERT ..... Enzyme Replacement Therapy
FD ..... Fabry Disease
KD ..... Kanzaki Disease
pNP ..... *para*-Nitrophenolate
pNP-α-Gal ..... *para*-Nitrophenol-α-galactose
pNP-α-GalNAc ..... *para*-Nitrophenol-α-N-acetylgalactosamine
SD ..... Schindler Disease

CHAPTER 1

INTRODUCTION

1.1 LSDs

There are approximately 50 diseases classified as Lysosomal Storage Disorders (LSDs), the majority of which are caused by deficiencies in lysosomal enzymes[1]. Perhaps one of the best understood LSDs is Fabry Disease (FD), first described 1898. FD stems from a patient's inability to produce sufficient functional quantities of the lysosomal enzyme α-Galactosidase A (α-GAL)[2]. Human α-GAL is responsible for catalyzing the hydrolysis of terminal α-galactose from oligosaccharides, glycoproteins, and glycolipids[3]. Individuals lacking functional α-GAL are unable to cleave the terminal galactose from (neutral) substrates (most notably globotriasylceramide (Gb-3)), leading to their accumulation[3]. The buildup of Gb-3 in the lysosome directly results in Fabry disease (FD) symptoms.

Over 400 mutations result in the condition, affecting approximately 1 in every 40,000 males[3,4]. Furthermore a number of female heterozygous carriers have been identified with symptoms of the X-linked recessive disorder, the manifestation of which is believed to be related to skewed X chromosome inactivation.[5] Common symptoms of FD include chronic pain, ocular opacities, skin lesions, liver and kidney impairment, vascular deficiencies and or cardiac deficiencies[4]. Enzyme Replacement Therapy (ERT), or repeated intravenous infusion of recombinant α-GAL in the form of either Fabrazyme (Genzyme Inc.) or Replagal (Shire), is the only approved treatment[6].

1.2 Problems with ERT

ERTs, or the infusion of recombinant enzyme for the treatment of LSDs, show adverse events including immunogenicity. Studies conducted on Fabrazyme and Replagal have shown that up to 88% of male patients receiving Fabrazyme and 56% of male patients receiving Replagal ERT develop IgG antibodies against the drugs[7,8]. Additionally 50-55% and 14% of patients receiving Fabrazyme and Replagal respectively also experience infusion reactions[9,10]. A clinical study further reported that out of 60 patients known to have experienced mild to severe Fabrazyme infusion reactions, 7 patients (8%) had developed IgE antibodies[9].

IgG antibody formation against Fabrazyme and Replagal is serious as it has been shown to have substantial neutralizing effects on α-GAL activity (as high as 74% in vitro)[11]. This could possibly lead to a loss of drug efficacy over time[11,12], consequently requiring an increase in dosage to overcome IgG antibody neutralization[11,12]. This may explain why Fabrazyme appears more efficacious than Replagal at its recommended dosage of 1.0mg/kg[9] (vs. Replagal 0.2 mg/kg[10]). However many of the symptoms commonly associated with Fabrazyme or Replagal ERT infusion reactions (chills, fever, acroparesthesias, dyspnea, etc.[9,12]) are also believed to result from the presence of these IgG antibodies[12]. Hence higher dosage requirements include the possibility of more severe infusion reactions, and equate to higher production costs. Furthermore over 1% of Fabrazyme ERT patients experience severe anaphylactic reactions[9]. Not surprisingly, most patients are administered anti-inflammatory drugs (e.g. acetaminophen) as pre-treatments to Fabrazyme infusion, and in some cases anti-histamines or steroids are also pre-administered when patients demonstrate a history of reactions[9,11].

Clinical studies indicate that Fabrazyme has a higher instance of causing IgG antibody formation as compared to Replagal[9,10,11], raising the question of whether the different glycosylation states or the different dosages are responsible for this phenomenon[11]. After market studies on the two drugs examining IgG antibody formation reported no statistical difference in the number of patients who developed IgG antibodies against either drug when the administered dosages were equal[11]. As the two recombinant polypeptide sequences are identical[13], these data suggest that the polypeptides (not their glycosylation) are responsible for IgG antibody formation. Further in support of this hypothesis, neutralizing IgG antibodies formed against Fabrazyme have proven to be equally as neutralizing against Replagal in vitro[12]. This leads us to ask why patient immune systems would react to an essentially WT α-GAL polypeptide, normally present in all healthy individuals, as foreign antigen after infusion.

One possible explanation centers on FD being a protein folding disorder[4]. Recent evidence implicates many FD causing mutations as potentially recognized by cellular quality control systems such as ERAD[14] (Endoplasmic Reticulum Associated Degradation), resulting in protein degradation and failed lysosomal trafficking. This explains why most male FD patients express almost no α-GAL[12]. Consequently these patients may never have established α-GAL self-tolerence[12] during innate immune system self/non-self differentiation. This hypothesis also explains why the majority of female FD patients do not develop IgG antibodies to α-GAL infusion[9, 11, 12], as almost all female FD patients are heterozygous for the X-linked recessive disorder[9, 11,12]. Hence these female patients likely retain α-GAL self-tolerance as they express at least some α-GAL due to their dominant *GLA* allele on their second X-chromasome.

1.3 α-N-Acetyl-Galactosaminidase

Structurally and catalytically similar to α-GAL, α-N-Acetylgalactosaminidase (α-NAGAL) is also a human lysosomal enzyme, and is responsible for the catalytic cleavage of terminal α-linked N-acetyl-galactosaminides from glycosylated substrates[15,16]. Deficiency of functional α-NAGAL results in the accumulation of glycosphingolipids and sialylated substrates, leading to the autosomal recessive disorder known as Schindler disease[16] (SD). Symptoms of SD include infantile neurodegeneration (group 1), adult onset mild retardation (group 2, also known as Kanzaki disease), or symptoms ranging from seizures to autistic behavior (group 3)[15,16]. Currently, no treatment for Schindler disease exists. Furthermore as SD symptoms are primarily neurological[15], it is unlikely ERT would prove successful in treating the disease, as any replacement enzyme must cross the blood brain barrier[17].

1.4 Solution to ERT Immune-Response Problems

The known immunogenicity problems associated with ERT for Fabry disease lead us to propose a novel approach. We hypothesize engineering a protein that patients already make, but with a new enzymatic activity. To the immune system this enzyme would appear as self, preventing immune response, but at the same time replace the missing enzyme's activity.

We have rationally engineered the active sites of two human enzymes α-GAL and α-NAGAL to have interconverted substrate specificities. Human α-GAL is normally responsible for the hydrolysis of terminal α-Galactoside[3,18], while human α-NAGAL is predominantly responsible for the hydrolysis of terminal α-GalNAc containing

substrates[16]. Both human α-GAL and α-NAGAL are normally found in the lysosome as homodimeric glycoproteins, and share 46% amino acid sequence identity[3,16] (figure 1). Crystal structures of human α-GAL and α-NAGAL solved in 2004[3] and 2009[16] respectively show that both proteins contain an N-terminal $(\beta/\alpha)_8$ barrel (which contains the 13 active-site residues), and a C-terminal β sandwich domain comprised of eight antiparallel β strands[3,16]. The N-terminal domains correspond to the catalytic domain, while the C-terminal domains have no known function[3,16]. Comparing the active sites of α-GAL and α-NAGAL shows that 11 of the 13 active site residues are conserved between the two enzymes (see appendix for active site residues). The different substrate specificities of the two enzymes are solely dictated by the two non-conserved active-site residues, E203/L206 (α-GAL), and S188/A191 (α-NAGAL).

Using site-directed PCR mutagenesis, we have engineered point mutations into *GLA* (α-GAL) and *NAGA* (α-NAGAL) generating two double mutants we call α-GAL^{SA} and α-NAGAL^{EL} respectively. In order to interconvert the substrate specificities of these two enzymes we have mutated α-GAL active-site residues Glu 203 to Ser and Leu 206 to Ala (E203**S**/L206**A**), and α-NAGAL active-site residues Ser 188 to Glu and Ala 191 to Leu (S188**E**/A191**L**). We hypothesized that these mutations should generate an α-NAGAL enzyme with α-GAL activity/substrate specificity (α-NAGAL^{EL}), and an α-GAL enzyme with α-NAGAL activity/substrate specificity (α-GAL^{SA}).

In this thesis, we show that these mutants maintain their respective WT immuno-reactive properties. Kinetic studies performed on both mutants and WT enzyme controls show that substrate specificities and activity were interconverted between the mutants. The data indicate that α-NAGAL^{EL} shares kinetic properties similar to WT α-GAL, and

that α-GAL^{SA} exhibits kinetic properties of an α-NAGAL enzyme. Western blots performed on both double mutants and WT enzymes with anti α-GAL and anti α-NAGAL IgG polyclonal antibodies show that both mutants maintain their respective WT parent enzyme's antigenicity.

We also determined four crystal structures of the α-GAL^{SA} mutant with either α-galactose, α-GalNAc, or the cryoprotectant glycerol (two structures) soaked into the active site. The crystal structures reveal the structure-activity relationship dictating substrate specificity between α-GAL and α-NAGAL. The crystallographic data also provide insight into why α-GAL^{SA} is less catalytically efficient than WT α-NAGAL. The data show that α-NAGAL^{EL} could be a viable alternative ERT for Fabry disease that could potentially avoid common immune-response issues associated with enzyme replacement therapy. [Michaelis-Menten kinetic studies and western blot data were obtained in collaboration with Matt Metcalf (University of Massachusetts Amherst) on the α-NAGAL^{EL} mutant (cloned, expressed, and purified by Matt Metcalf). Abby Guce and Nat Clark (University of Massachusetts Amherst) also participated in this project, cloning and expressing WT α-GAL and α-NAGAL respectively.]

CHAPTER 2

RESULTS

2.1 PCR Mutagenesis

Point mutations were introduced into *GLA* and *NAGA* via PCR mutagenesis (Methods). The PCR mutagenesis strategy uses mismatches designed into the forward PCR primer to introduce point mutations into the gene of interest. The majority of the DNA amplified during PCR mutagenesis contained the desired point mutations. Successful PCR mutagenesis was analyzed via agarose gel electrophoresis stained with EtBr (figure 2). Restriction digest controls of uncut super-coiled plasmid and single-digest linear plasmid were subjected to agarose gel electrophoresis alongside the mutagenesis products. Figure 2 illustrates that PCR amplification of pIB-V5-His-TOPO-α-GAL-1& 4 (parallel experiments) occurred, using primers designed with the desired mismatched bases. The starting concentration of plasmid for each reaction was 0.2 pg/μL and is not visible on an agarose gel. The PCR products running at 4.8 kb match the size of control plasmid linearized via single restriction enzyme digestion (lane 11, lane 3 single-digest control did not appear for unknown reasons). The data indicate that the PCR mutagenesis reactions yielded products of the appropriate size expected for linearized pIB/V5-His-TOPO-α-GAL^{SA}. Mutagenesis products from lanes 6 and 12 demonstrate the strongest amplification, and were chosen for ligation and transformation.

2.2 Ligation and Transformation

PCR products from lanes 6 and 12 were ligated with T4 DNA Ligase, and used to transform both TAM-1 and NEB *E. coli* cells in tandem experiments (on ampicillin plates). Isolated DNA was subjected to restriction enzyme digestion to assay for plasmid integrity. Each isolated plasmid was subjected to a single (*HinDIII*) and double (*HinDIII + XhoI*) digestion. If intact, the single-digest reaction should linearize the 4.8 kb plasmid DNA, while the double-digestion should cut around the 1.2 kb α-GAL *GLA* insert. Restriction enzyme digestion was analyzed via agarose gel electrophoresis. The agarose gel (figure 3) shows that all 6 digested α-GAL^{SA} mutant candidates contain the 1.2 kb *GLA* insert, indicating that all 6 isolated plasmids are intact.

2.3 DNA Sequencing

Sequencing data on the 6 isolated plasmids show that 1 of the 6 plasmids contained the desired point mutations. Part of the sequence chromatogram highlighting the desired codon mutations (**GA**G → **TC**G (E203S) and **CT**T → **GC**T (L206A)) is shown in figure 4, aligned to the WT *GLA* sequence.

2.4 Stable Cell Line

After DNA sequencing data verified the presence of the α-GAL^{SA} mutations, Invitrogen High-5 (Tn5) and Sf21 insect cells were transfected with the α-GAL^{SA} construct (figure 5). Stable cell lines were generated via antibiotic selection with blasticidin (figure 6). The α-GAL^{SA} construct contains a blasticidin resistance gene, and cells that integrate the vector into their genomes should become blasticidin resistant.

Protein expression was analyzed using western blots (figure 7). Two western blots were performed, one probing with polyclonal anti-α-GAL, and the other with polyclonal anti-hexahistidine antibodies. Both western blots show that α-GAL^{SA} expressed in High-5 insect cells. Coomassie stained protein appears between the 56 kDa and 43 kDa MW markers, matching the 50 kDa predicted size for glycosylated α-GAL subjected to SDS-PAGE. Sf21 insect cells did not express any detectable protein. Sf21 cells are more commonly used for baculovirus amplification, rather than protein expression[19].

2.5 Large-scale Expression and Purification

An overview of the α-GAL^{SA} purification process is presented in figure 8. Large-scale suspension cultures of the α-GAL^{SA} stable-cell line were grown to a density of 5-6 x 10^6 cells/ml. α-GAL^{SA} contains a secretion signal and is secreted into the media. 8 liter cultures were subjected to centrifugation to pellet the cells, and the supernatant was collected. Collected supernatant was concentrated and buffer exchanged using a prep/scale tangential flow Millipore cartridge (MW cutoff of 10 kDa). This was done to remove contaminant commonly present in SFX media that removes Ni from Ni-Sepharose resin. The supernatant was concentrated by tangential flow filtration to a volume of 1 liter for chromatography (figure 9).

2.6 Ni Affinity Chromatography 1

A liter of concentrated retentate was loaded onto a prepacked 5 ml Ni-column at a flow rate of 2 ml/min using a Bio-Rad Biologic Duo-Flow FPLC (Methods). A 25 ml

wash step (Ni-Wash Buffer) preceded a very shallow linear elution gradient of 0 to 70% Ni-Elution Buffer over a volume of 300 ml. Fractions were collected every 2 ml. The UV 280 nm absorbance chromatogram (generated during chromatography) shows a broad peak between an elution volume of ~120-240 ml (fractions 60-120) (figure 10). This broad peak is preceded by a larger peak between an elution volume of 50-100 ml (fractions 23 – 55), representing a common large molecular weight contaminant.

α-GAL^{SA} fractions were monitored using SDS-PAGE (figure 10). The SDS gel shows the majority of pure α-GAL^{SA} eluting between fractions 80-137. Pure α-GAL^{SA} fractions were pooled and concentrated. Pure α-GAL^{SA} was stored in 10 mM NaH_2PO_4 at pH 6.5. The SDS gel shows that fractions 53-79 also contain α-GAL^{SA} protein, but that these fractions contain contaminants that eluted with the protein of interest. Hence, these fractions were pooled separately and subjected to an additional Ni affinity purification, along with the supernatant flow-through from this first Ni-purification.

2.7 Ni Purification 2

An identical protocol to the one used for the first Ni affinity purification was used for the second, and fractions were similarly monitored via SDS-PAGE. The 280 nm absorbance chromatogram and the corresponding SDS gel are shown in figure 11. A large molecular weight contaminant eluted between fractions ~25-60. The SDS gel shows that pure α-GAL^{SA} eluted between fractions 70 and 118. The area corresponding to these fractions is circled in blue in figure 11. Pure α-GAL^{SA} was pooled and concentrated, and stored in 10 mM NaH_2PO_4 at pH 6.5. α-GAL^{SA} protein from the first

Ni affinity purification was pooled with pure protein from the second and further concentrated to 6.21 mg/ml. Remaining impure α-GAL^{SA} fractions (fractions 56-69) were further purified using anion exchange chromatography.

2.8 Anion Exchange Chromatography

See methods for the anion exchange chromatography protocol. Eluted fractions were monitored via SDS-PAGE and UV 280 nm absorbance (figure 12). The SDS gel indicates that pure protein matching the predicted size of α-GAL^{SA} appears between the 56 kDa and 43 kDa markers (fractions 60-137). Fractions 70-137 were pooled, concentrated, and stored in 10 mM NaH_2PO_4 at pH 6.5. Pure α-GAL^{SA} from the two Ni affinity chromatography purifications and the single anion exchange chromatography purification was pooled, and further concentrated to a concentration of ~7 mg/ml.

2.9 Immunogenicity

Figure 13 depicts the four enzymes (α-GAL, α-GAL^{SA}, α-NAGAL, α-NAGAL^{EL}) analyzed with SDS-PAGE, and stained with Coomassie Brilliant Blue. The SDS gel shows that α-GAL and α-GAL^{SA} both run at about 50 kDa in lanes 1 and 2 respectively, and that both α-NAGAL and α-NAGAL^{EL} run at about 52 kDa in lanes 3 and 4 respectively. This result is as expected, as each mutant is only two amino acid residues dissimilar from its respective WT enzyme, and accordingly should not display a large difference in mass. Additionally all bands on the SDS gel appear equally intense, showing the four enzymes are at approximately equal concentrations.

Western blots of α-GAL and α-NAGAL along with their respective mutants, probing with IgG polyclonal anti-α-GAL and polyclonal anti α-NAGAL antibodies, are shown in figure 13. Only α-GAL and α-GAL^{SA} react with IgG anti α-GAL antibodies, and only α-NAGAL and α-NAGAL^{EL} react with IgG anti α-NAGAL antibodies. These data show that α-GAL^{SA} and α-NAGAL^{EL} maintain their respective WT enzyme's antibody epitopes, and show that the mutants and their respective WT enzymes do not cross-react with each other's antibodies.

2.10 pNP Activity Assays

To measure enzyme activity, kinetics, and substrate specificity, the enzymatic hydrolysis of the synthetic substrates pNP-α-Gal or pNP-α-GalNAc was monitored at an absorbance wavelength of 400nm at 37°C. The pNP assays function as shown below, (for detailed protocol see appendix A):

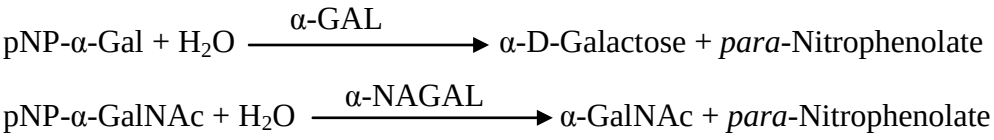

2.11 Optimal pH and Buffer Conditions

Optimal pH and buffer conditions for α-GAL^{SA} activity were experimentally determined by measuring specific enzyme activity at varying pH conditions, in either citrate or phosphate buffer. The plot of α-GAL^{SA} activity vs. pH (from pH 3 to 9.8) in either citrate or phosphate buffer shows that α-GAL^{SA} activity was optimal at pH 4.5, in citrate buffer (figure 14). Similar activity assays were performed (by Abby Guce and

Matt Metcalf) on α-GAL, Fabrazyme, α-NAGAL, and α-NAGAL^{EL} (data not shown), also indicating that pH 4.5 and citrate buffer show the optimal activity of these enzymes. pH 4.5 is representative of lysosomal pH[20].

2.12 Specific Activity

Enzyme activity and substrate specificity of Fabrazyme (recombinant human α-GAL from CHO cells, Genzyme Inc.), α-GAL^{SA}, and human α-NAGAL (produced in insect cells) was measured. The assay involves incubating the enzyme of interest with synthetic substrate for 10 min, then quenching the reaction with borate buffer (pH 9.8). The amount of para-nitrophenol hydrolyzed from synthetic substrate by each enzyme is then measured by absorbance wavelength of 400nm. Absorbance measurements were used to calculate the amount of normalized activity using Equation 1 (appendix).

The results (figure 15) show that the catalytic activity of α-GAL^{SA} resembles that of α-NAGAL more closely than that of α-GAL. α-GAL^{SA} and α-NAGAL both demonstrate an affinity for hydrolyzing pNP-α-GalNAc that is about 7 times greater than their affinity to hydrolyze pNP-α-Gal. The data indicate that α-GAL^{SA} is about 3 times less active than WT α-NAGAL. To more thoroughly understand the catalytic properties of α-GAL^{SA}, Michaelis-Menten kinetic measurements on α-GAL^{SA}, α-NAGAL^{EL}, and WT enzyme controls were performed.

2.13 Michaelis-Menten Kinetics

Michaelis-Menten kinetic data on the four enzymes (α-GAL, α-GAL^{SA}, α-NAGAL, and α-NAGAL^{EL}) were measured to quantify changes in substrate specificity

(k_{cat}/K_m) and catalytic efficiency (k_{cat}) relative to WT enzyme controls. To obtain kinetics data on these enzymes, the amount of *para*-nitrophenol hydrolyzed from synthetic substrates pNP-α-Gal or pNP-α-GalNAc was measured with respect to time, at different substrate concentrations (methods). The data (figure 16) indicate that both α-GAL^{SA} and α-$NAGAL^{EL}$ exhibit interconverted substrate specificities that more closely reflect specificities resembling that of WT α-NAGAL, and α-GAL respectively.

α-GAL^{SA}: α-GAL^{SA} specificity for α-GalNAc is about 40 times greater than its specificity for α-Gal, its natural substrate. The results show that α-GAL^{SA} exhibits a k_{cat} of about 21.5 sec^{-1} against pNP-α-GalNAc, while α-NAGAL exhibits a k_{cat} of about 15.1 sec^{-1} against the same substrate. This shows that α-GAL^{SA} is as efficient as α-NAGAL at catalyzing the hydrolysis of pNP-α-GalNAc once substrate has reached the active site. However, the K_m of α-GAL^{SA} (21.0 mM) is markedly higher than that of WT α-NAGAL (K_m=0.68 mM) against the same pNP-α-GalNAc substrate. Hence, the specificity constant (k_{cat}/K_m) of α- GAL^{SA} against pNP-α-GalNAc is about 20 fold lower than that of α-NAGAL, being ~1.03 (mM^{-1} sec^{-1}) vs. 22.4 (mM^{-1} sec^{-1}) respectively.

α-$NAGAL^{EL}$: The *NAGA* mutations have completely eliminated any of the mutant's native α-NAGAL activity, as attempts to measure kinetics against pNP-α-GalNAc yield measurements indistinguishable from blank readings. This result is comparable to α-GAL, which also shows no activity toward pNP-α-GalNAc. The K_m of α-$NAGAL^{EL}$ against pNP-α-Gal is close to that of α-GAL, being 7.6 mM and 6.9 mM respectively. The data show that α-$NAGAL^{EL}$ catalyzes the hydrolysis of pNP-α-Gal with a catalytic efficiency (k_{cat}) of 13.7 sec^{-1}, which is less than three times lower than the k_{cat} α-GAL displays against pNP-α-Gal, which is 37.8 sec^{-1}. Accordingly, the specificity

constant (k_{cat}/K_m) of α-NAGAL^{EL} against pNP-α-Gal is only about three times lower than that of α-GAL, being 1.8 (mM^{-1} sec^{-1}) and 5.5 (mM^{-1} sec^{-1}) respectively. Hence, the data show that the *NAGA* mutations converted the substrate specificity of α-NAGAL to more closely reflect the substrate specificity of human α-GAL.

2.14 X-Ray Crystallography

Four α-GAL^{SA} crystal structures were determined with either α-galactose, α-GalNAc, or glycerol bound to the enzyme active site. The structures allow us to better understand the nature of how the *GLA* mutations alter substrate specificity of the enzyme. Crystallization screens were set up based on previous α-GAL crystallization conditions, using the hanging drop vapor diffusion method.

Conditions yielding crystals contained a reservoir solution of 8% or 12% polyethylene glycol (PEG) 8000, 22 mM $Mg(OAc)_2$, and 100 mM Sodium Cacodylate pH 6.5. Photographs of crystals obtained with these reservoir solutions are shown in figure 17. Crystals obtained with a reservoir solution of 12% PEG 8K, etc., initially yielded 500 μm crystals showing only two-dimensional growth with fraying (figure 17 D). These crystals were not suitable for data collection. However, a few crystals of acceptable quality (figure 17, E) were later obtained from this reservoir solution when macroseeding techniques were employed, and used for data collection. Overall, of the 24 conditions initially screened, two conditions yielded diffraction quality crystals.

Crystals were harvested stepwise from their reservoir solutions, and ligand-soaked (with α-Gal or α-GalNAc), before being transferred into a 20% glycerol based cryoprotectant. Crystals were flash cooled with liquid nitrogen, and then transferred to a

gaseous stream of liquid nitrogen at 100˚ K for X-ray diffraction screening. Screening was done in-house using a Rigaku MSC RUH3R X-ray generator, and diffraction images were digitally detected using Raxis IV++ detector. The crystal from figure 17 (B) was subjected to an exposure time of 5 min. The diffraction image shows that the crystal lattice is consistent with that of protein, exhibits non-overlapping spot shape, and has a low mosaicity. Diffraction data was collected at the Brookhaven National Laboratory's X6A beamline, and at Argonne National Laboratory's NECAT 24-ID-C beamline. A collection image is shown in figure 18 (B), taken with an exposure time of 30 seconds at BNL X6A beamline.

Crystallographic data (table 1) show that crystals obtained from a reservoir solution of 8% or 12% PEG 8K etc., grew with $P2_12_12_1$ or $C222_1$ space group symmetry, respectively. Diffraction images were processed using HKL2000[21] and phased by molecular replacement in AMoRe[24], or by Fourier synthesis with human α-GAL mutant D170A (PDB: 3HG3)[21]. Atomic models were built using the program O[25], and refined with REFMAC5[24]. Ramachandran plots were computed using PROCHECK[26], and coordinates were superimposed using LSQMAN[27]. The four structures show a range in resolution from 2.1-3.1 Å, with the α-GalNAc bound structure exhibiting the best resolution at about 2.1 Å, and the best R_{work}/R_{free} at 17.62/21.82. Ramachandran plots of the four structures show ~90% of the residues fall in the favored region.

Superimposition of α-GAL^{SA} and α-NAGAL by 290 Cα atoms in their $(\beta/\alpha)_8$ barrels shows an RMS deviation of 0.58 Å (figure 19). The α-GalNAc ligands superimpose almost exactly, with the 15 atoms in the GalNAc ligands having an RMS deviation of 0.38 Å. This is quite remarkable, as only 46% of the residues are conserved

between the two enzymes. Superimposition of galactose bound α-GAL^{SA} with WT α-GAL reveals the active sites are similar, but that the two structures demonstrate variation in their active sites beyond the E203S/L206A substitutions. The data show that the D170 catalytic nucleophile moves, occupying the space vacated by the E203S substitution. This is likely responsible for the diminished catalytic efficiency exhibited by α-GAL^{SA}, as D170 participates in important hydrogen bonding contacts with active site residues Y134 and Y207.

Two separate crystal structures of α-GAL^{SA} were determined with the glycerol cryoprotectant soaked into the active site. Each one of the two crystals (having $P2_12_12_1$ or $C222_1$ space group symmetry) contained two monomers of α-GAL^{SA} per asymmetric unit. This allowed us to compare four crystallographically independent glycerol-bound active sites (figure 19), which showed that one of the four monomers was unique. Significant differences included the glycerol cryoprotectant binding in an alternate orientation, an alternate R227 side chain rotamer position, and the movement of the β6-α6 loop harboring residue D231, the catalytic acid-base. This novel reorganization of the active site in two of the four α-GAL^{SA} structures indicates that the E203S/L206A substitutions have reduced the structural integrity of the enzyme, likely lowering its stability and contributing to the low catalytic efficiency of this mutant.

CHAPTER 3

DISCUSSION

88% of patients receiving recombinant α-GAL enzyme replacement therapy for Fabry disease develop IgG antibodies against the drug. Since Fabry disease is an X-linked recessive disorder, male Fabry patients only harbor a single defective copy of *GLA*. In most male patients this results in failed trafficking of α-GAL to the lysosome[4]. It is believed that most male FD patients develop IgG antibodies towards α-GAL because they have never become immunologically self-tolerized to the enzyme. In line with this hypothesis, heterozygous female FD patients do not mount IgG responses toward the enzyme[9,11,12]. Hence, Fabry patients would experience a greater clinical benefit if a non-immunogenic enzyme replacement therapy for FD were developed.

Western blots probing with anti α-GAL and α-NAGAL antibodies show that α-GAL and α-GAL^{SA} only react with anti α-GAL antibodies, while α-NAGAL and α-NAGAL^{EL} only react with anti α-NAGAL antibodies. Although α-GAL and α-NAGAL exhibit similar folds and share 46% sequence identity, the sequences show enough variation to prevent cross-reactivity between the two proteins. Hence, we have shown that α-NAGAL^{EL} exhibits substrate specificity similar to that of α-GAL, yet maintains its α-NAGAL parent enzyme antigenicity. Although less catalytically efficient than α-GAL, α-NAGAL^{EL} could provide a potential efficacy gain over either Fabrazyme or Replagal if the reduced immunogenicity of the mutant eclipses its approximate three fold reduction in activity compared to WT α-GAL. In line with this hypothesis, Sakuraba and colleagues generated a protein similar in design to α-NAGAL^{EL} (except expressed in

CHO cells)[22]. They showed that administering α-NAGAL^{EL} to a mouse model of FD effectively reduced Gb-3 levels in the lysosome when compared to control mice[22].

Likewise, the substitutions in α-GAL^{SA} generated an enzyme with specificity for the α-GalNAc substrate, while retaining the mutant's WT enzyme immunogenicity. The crystal structures show that by converting the larger residues E203 and L206 to S and A respectively, the active site of the enzyme was enlarged enough to accommodate the bulkier N-acetyl group at the 2-position of the α-GalNAc sugar ring. This N-acetyl group at the 2-position on the sugar ring is normally occluded from the active site of WT α-GAL by steric clashes, allowing α-GAL and α-NAGAL to discriminate between their substrates.

The crystal structures of α-GAL^{SA} indicate that the mutant has a more dynamic and flexible active site than WT α-NAGAL. Although enlarging the α-GAL^{SA} active site via the shortening of residues E203 and L206 in the β5-α5 loop did facilitate the accommodation of the bulkier α-GalNAc substrate, it simultaneously removed some packing interactions provided by these residues. The R227 side chain moves into the space previously occupied by the side chain of E203, and the β6-α6 loop (D231) move into the space previously occupied by the side chain of L206 in the glycerol bound structure. A more dynamic active site is further supported by the higher atomic B-factors in the β6-α6 loop in the glycerol-soaked structure, indicating higher active site mobility.

It is perplexing that α-GAL^{SA} and α-NAGAL are not more catalytically comparable given that they share a near identical active site constellation. However α-NAGAL likely provides additional steric support to its active site via residues Y215 and F232, which participate in van der Waals interactions stabilizing the β6-α6 loop (which

moves in the α-GAL^{SA} structure). α-GAL^{SA} lacks this additional stability, as its equivalent residues F229 and T246 do not interact. Hence it is possible that the catalytic efficiency of α-GAL^{SA} could be improved by making an α-GAL^{SA} mutant with Y and F residues substituted for F229 and T246, respectively. This mutant's active site may prove to be less dynamic, yet still be able to accommodate α-GalNAc, increasing its catalytic efficiency.

CHAPTER 4

SUMMARY

We have successfully engineered the E203S/L206A amino acid substitutions into the α-GAL protein via PCR mutagenesis, and expressed and purified the α-GAL^{SA} mutant from insect cells. We have shown that α-GAL^{SA} exhibits kinetic properties resembling that of WT α-NAGAL more so than that of WT α-GAL. We have shown that the α-NAGAL^{EL} mutant exhibits kinetic properties close to that of α-GAL, and has completely lost the ability to catalyze the hydrolysis of pNP-α-GalNAc. Both α-GAL^{SA} and α-NAGAL^{EL} retain their respective WT enzyme antigenic properties, and more importantly we have demonstrated that the mutants do not cross react with each other's antibodies. The crystallographic data reveal the mechanism by which substrate specificity is interconverted between these two enzymes, and provides insight into why the mutants exhibit reduced catalytic efficiency compared to WT enzymes. α-NAGAL^{EL} may prove fruitful as an alternative enzyme replacement therapy for Fabry disease in patients where adverse immune reactions to the current treatment is an issue.

Rational protein design has always been a difficult process. For example, the conversion of trypsin to chymotrypsin activity requires 11 residue substitutions[23]. Here we have shown and reaffirmed that a rational design approach can be successfully used to design proteins with new enzymatic function. This technique may prove to be a useful approach in designing new enzyme replacement therapies as treatments for a variety of diseases where immune response may be an issue.

CHAPTER 5

METHODS

5.1 PCR Mutagenesis

The human α-galactosidase A gene (*GLA*, Accession code: NM_000169.2) was cloned into a commercial pIB/V5-His-TOPO cloning vector (Invitrogen Life Sciences Inc., Carsbad CA, USA). The pIB/V5-His-TOPO-α-GAL construct encodes the 429 amino acid residue α−Galactosidase A protein, including its 31 amino acid signal sequence, and a 6xHis tag at the C-terminus of the enzyme. The construct also contains ampicillin and blasticidin antibiotic resistance genes (figure 2). Point mutations in *GLA* were introduced to convert α-GAL E203 to S and L206 to A (α-GAL^{SA}). α-GAL^{SA} mutations were made using Finnzyme's Phusion Site-Directed Mutagenesis kit (Finnzyme, USA) and mutagenesis primers designed as described in the Finnzyme protocol (appendix A). Primers were purchased from Integrated DNA Technologies Inc. (1710 Commercial Park, Coralville IA, USA). Forward primer: 5′-/5PO_4/G TAC TCC TGT **TC**G TGG CCT **GC**T TAT ATG TGG CCC-3′, and reverse primer: 5′-/5PO_4/CAC AAT GCT TCT GCC AGT CCT ATT CAG GGC-3′, were used to introduce the E203S/L206A mutations into *GLA* (mutated nucleotides are shown in bold). Matt Metcalf used PCR mutagenesis to introduce point mutations into *NAGA* generating the α-NAGAL^{EL} mutant; Forward PCR primer: 5'-/5PO_4/CGG CCT CCC CCC AAG GGT GAA CTA-3', and reverse PCR primer: 5'-/5PO_4/CC TTC ATA G**AG** TGG CCA **CTC** GCA GGA GAA-3'.

5.2 Ligation, Transformation, and Sequencing

The PCR mutagenesis product was ligated and transformed via the heat shock method into NEB *E. coli* competent cells grown on LB ampicillin (100 μg/ml) plates. Ampicillin resistant colonies were re-streaked, and subsequently inoculated into 50 ml LB Amp media (100 μg/ml) for DNA amplification. PIB/V5-His-TOPO-α-GAL^{SA} mutant plasmid was isolated and the presence of the α-GAL^{SA} mutation confirmed via sequencing data obtained from Genewiz sequencing services (Genewiz Inc., USA).

5.3 Transfection

The pIB-V5-His-TOPO-α-GAL^{SA} stable cell line construct was transfected into Invitrogen High-Five insect cells by adding 1.8 μg of DNA to 36.4 μl of Cellfectin reagent (Invitrogen, USA), along with 1.8 ml Hyclone-SFX serum-free media (Thermo Fisher Scientific Inc.). The mixture was incubated for 15 min, and then added it to a T-25 flask seeded with 3.6 x 10^6 cells grown with Hyclone-SFX media. Cells were rocked for 6 hours in the presence of the transfection mixture, before 5 ml of fresh SFX media was added. Cells were allowed to reach confluency over 2 days. Transfections were subsequently passaged in SFX media containing blasticidin at a concentration of 100 μg/ml for two weeks facilitating selection, after which cells were passaged only with SFX media. Protein expression was assayed via western blotting using polyclonal anti-hexahistidine IgG (Qiagen Inc., USA), and polyclonal anti-α-Galactosidase IgG (Genetel Laboratories LLC, USA) primary antibodies. Blots were developed using 1-Step™ NBT/BCIP (Thermo Fisher Scientific Inc., USA) after treatment with the appropriate AP

conjugated secondary antibody, anti-mouse IgG (Sigma-Aldrich Inc., USA), or anti-chicken IgY (Genetel Labs LLC) respectively.

5.4 Large Scale Expression and Purification of α-GAL^{SA}

Large scale (8, 1L cultures) stable cell line suspension cultures of the α-GAL^{SA} mutant cell line were grown at 37°C, to a density of ~5-6 x 10^6 cells/ml for approximately 3 days. Supernatant was collected via centrifugation, and NaN_3 added to a final concentration of 0.01% to prevent bacterial growth. Supernatant was concentrated and buffer exchanged with Ni Wash Buffer (20 mM NaH_2PO_4, 0.5 M NaCl, 20 mM Imidazole, pH 7.5) using a Prep/Scale tangential flow filtration cartridge (Millipore) with a 10 kDa MWC. Retentate was loaded onto a prepacked 5 ml Ni Sepharose 6 Fast Flow column (GE Healthcare) equilibrated with binding buffer at a flow rate of 2 ml/min using a Bio-Rad Biologic Duo-Flow FPLC (Bio-Rad Laboratories Inc., USA). Eluted α-GAL^{SA} was monitored using SDS-PAGE, and pure fractions were pooled and concentrated using Sartorius Vivaspin concentrators with a MWC of 10 kDa, and stored in 10 mM NaH_2PO_4.

Any remaining impure fractions eluted from this Ni affinity column purification, along with the flow-through supernatant, were pooled and subjected to a second Ni affinity purification using an identical protocol as the one applied to the first Ni purification. Again, fractions were monitored using SDS-PAGE, pure fractions were pooled and concentrated using Sartorius Vivaspin concentrators with a MWC of 10 kDa, and stored in 10 mM NaH_2PO_4.

Any remaining impure fractions from this second Ni purification were dialyzed with anion (Q) Wash Buffer (20 mM Bis-TRIS, pH 7.5) using a dialysis membrane with a MWC of 10 kDa . Dialyzed fractions were loaded onto a 5.0ml UNO^{TM} Q anion exchange column (Bio-Rad, USA) at a flow rate of 1ml/min. Protein was eluted using Q Elution Buffer (20 mM Bis-TRIS, 500 mM NaCl, pH 7.5) over a volume of 350 ml. Eluted α-GAL^{SA} protein was monitored using SDS-PAGE, and pure protein was pooled and concentrated using Sartorius Stedim Biotech Vivaspin concentrators with a MWC of 10 kDa, and stored in 10 mM NaH_2PO_4 at pH 6.5. Pure α-GAL^{SA} protein from the two Ni and one Q purification were subsequently pooled and further concentrated to ~7 mg/ml.

5.5 Michaelis Menten Kinetics

In all experiments the enzymatic hydrolysis of either synthetic substrates *para*-nitrophenyl-α-Galactose (pNP-α-Gal) (Toronto Research Chemicals Inc., Canada) or *para*-nitrophenyl-2-acetamido-2-deoxy-α-D-galactopyranoside (pNP-α-GalNAc) (Toronto Research Chemicals Inc., Canada) was monitored at an absorbance of 400 nm at 37º C. An extinction coefficient of 18.1 mM^{-1} cm^{-1} was used. The amount of *para*-nitrophenolate cleaved by the enzyme of interest with respect to time at varying substrate concentrations was used as a measure of the rate of enzyme activity. The amount of product cleaved at each substrate concentration was plotted against time yielding initial velocities (V_0) for each substrate concentration. V_{max} and K_m values were calculated using weighted non-linear least squares regression curve fittings of initial velocity as a

function of substrate concentration according to the Michaelis-Menten equation (Equation 2) using KaleidaGraph.

$$V_0 = (V_{max}[S])/(K_m + [S]) \qquad (2)$$

To measure rates, 140 uL of either pNP-α-Gal or pNP-α-GalNAc at varying substrate concentrations ([pNP-α-Gal]: 0.047 mM – 50.0 mM; [pNP-α-GalNAc]: 0.047 mM – 50.0 mM) were incubated with 10 uL of enzyme ([WT-α-GAL]: ~0.025 mg/ml, [α-GAL^{SA}]: ~0.1 mg/ml, [α-$NAGAL^{EL}$]: ~0.05 mg/ml, [WT α-NAGAL]: ~0.025 mg/ml) at 37º C to a final volume of 150 uL. (For a blank measurement a 10 μL aliquot of the reaction mixture was quenched in 290 μL of borate buffer (200 mM Na_3BO_3, pH 9.8) immediately after mixing enzyme and substrate.) 10 uL aliquots were subsequently quenched in 290 μL borate buffer every min constituting experimental time points. All experiments were performed using clear flat bottom 96 well plates (Fisher). Absorbance at 400 nm was measured using a Molecular Devices SpectraMax 5 plate reader and data was collected using Soft Max Pro™. All stock pNP-α-GalNAc and pNP-α-Gal solutions were dissolved in citrate buffer (100 mM Citric Acid, 100 mM NaH_2PO_4, pH 4.5), and all enzyme solutions diluted in 100 mM Citric Acid, 100 mM NaH_2PO_4, 0.1% BSA, pH 4.5. All kinetic experiments were preformed in triplicate each of by two separate experimenters.

5.6 Crystallography

Crystals were grown using the hanging drop vapor diffusion method and macroseeding techniques were employed to increase the size of crystals. Crystals grown

with $P2_12_12_1$ space group symmetry grew from a crystallization solution that contained a reservoir of 8.0% Polyethylene Glycol 8000 (PEG 8k), 22 mM $Mg(OAc)_2$, and 100 mM NaCacodylate pH 6.5. Drops were set up using a 1:1 mixture of reservoir solution and stock α-GAL^{SA} protein solution (7.0 mg/ml) in 10 mM NaH_2PO_4, which yielded poor diffraction quality crystals. These crystals were then crushed and used to seed a pre-equilibrated 1:1 mixture of reservoir solution to stock protein solution and incubated at 20º C for about 2 weeks. A number of these crystals were soaked in an α-galactose solution (8.0% PEG 8k, 22 mM $Mg(OAc)_2$, 100 mM NaCacodylate pH 6.5, 200 mM galactose), prior to harvesting with 8.0% PEG 8k, 22 mM $Mg(OAc)_2$, 100 mM NaCacodylate pH 6.5, and 20% Glycerol before the crystals were then flash cooled in liquid nitrogen. A number of small crystals were also harvested into buffer containing 8.0% PEG 8k, 22 mM $Mg(OAc)_2$, 100 mM NaCacodylate pH 6.5, and 20% glycerol before being flash cooled in liquid nitrogen.

Crystals grown in the $C222_1$ space group were grown using the hanging drop vapor diffusion method. Crystals were grown using a reservoir solution of 12.0% PEG 8k, 22 mM $Mg(OAc)_2$, and 100 mM NaCacodylate pH 6.5. Drops were set up using a 1:1 mixture of reservoir solution to stock α-GAL^{SA} protein solution in 10mM NaH_2PO_4, pH 6.5. Crystal were soaked in either an α-GalNAc, or α-Gal solution (12.0% PEG 8k, 22 mM $Mg(OAc)_2$, 100 mM NaCacodylate pH 6.5, 200 mM α-GalNAc or 200 mM α-Gal) prior to harvesting with 15.0% PEG 8k, 22 mM $Mg(OAc)_2$, 100 mM Na Cacodylate pH 6.5, and 20% glycerol. Crystals were subsequently flash cooled with liquid nitrogen.

5.7 X-ray Data Collection and Refinement

Several crystals were screened in house using a Rigaku MSC RU-H3R X-ray generator. Crystals were screened using an exposure time of 5 min to 1 hour under a stream of gaseous liquid nitrogen at 100° K, and data detected using a RAxis IV++ detector. Promising crystals were transported to the Brookhaven National Laboratory Synchrotron Light Source X6A beamline and the Argonne National Laboratory's NECAT 24-ID-C beamline, where X-ray diffraction data was collected under a stream of gaseous nitrogen at 100º K. Diffraction images were scaled and integrated using HKL2000[21]. The structures were phased by molecular replacement in AmoRe[24], or by Fourier synthesis with human α-GAL mutant D170A (PDB: 3HG3)[21]. Atomic model building was preformed with the program O[25], and REFMAC5[24] was used for refinement. Ramachandran plots were computed using PROCHECK[26], and coordinates were superimposed using LSQMAN[27].

CHAPTER 6

FIGURES

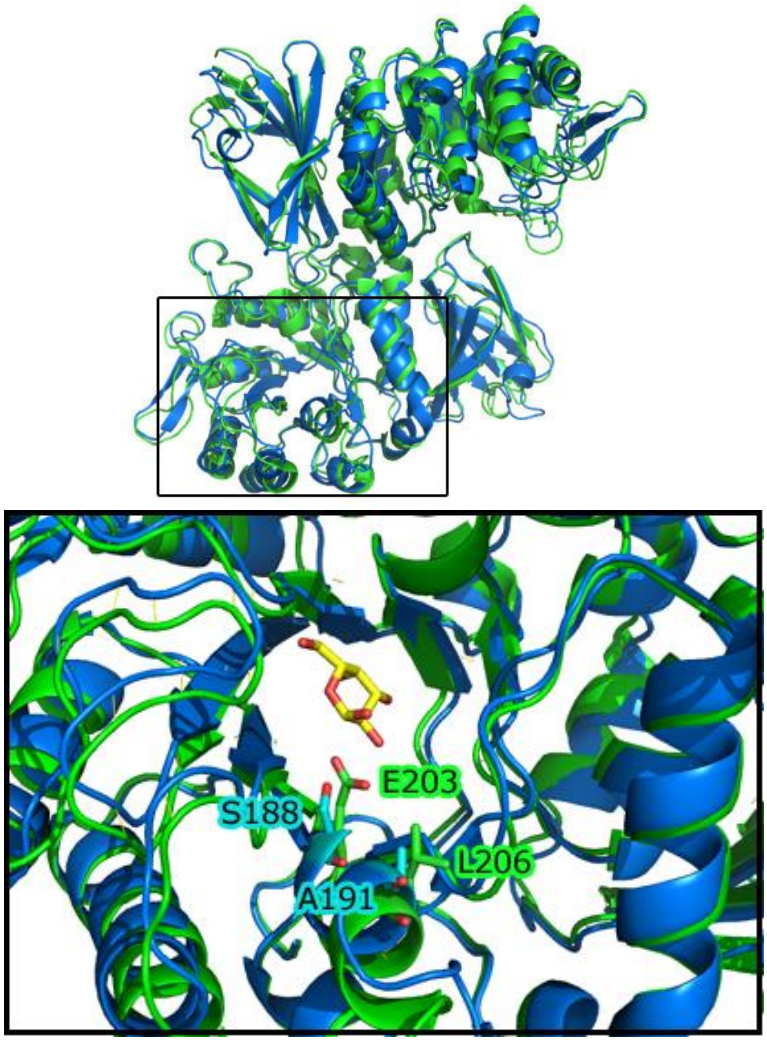

Figure 1: Structure of Human α-GAL and α-NAGAL. (Above) Structure of WT human α-GAL (green) at 2.3 Å resolution (3HG2)[19] superimposed on WT human α-NAGAL (blue) at 1.9 Å resolution (3H55)[16] (glycosylation omitted). The homodimeric glycoproteins are homologous. Although sharing only 46% amino acid sequence identity, similarity between their secondary structure is extensive[16,19]. Notice that both enzymes contain an N-terminal $(\beta/\alpha)_8$ barrel harboring the catalytic active site, and a C-terminal β sandwich domain composed of eight antiparallel β strands[16,19]. (Below) Blown up view of the N-terminal $(\beta/\alpha)_8$ barrel. Both enzymes contain a 13 residue active site. 11 of 13 active site residues are conserved between the two glycoproteins. Shown in sticks, the two non-conserved active site residues E203/L206 (α-GAL), and S188/A191 (α-NAGAL). The normal WT α-GAL ligand (α-galactose) is shown within the active site in yellow. Images were generated using PyMOL molecular viewer (v1.1, DeLano Scientific LLC).

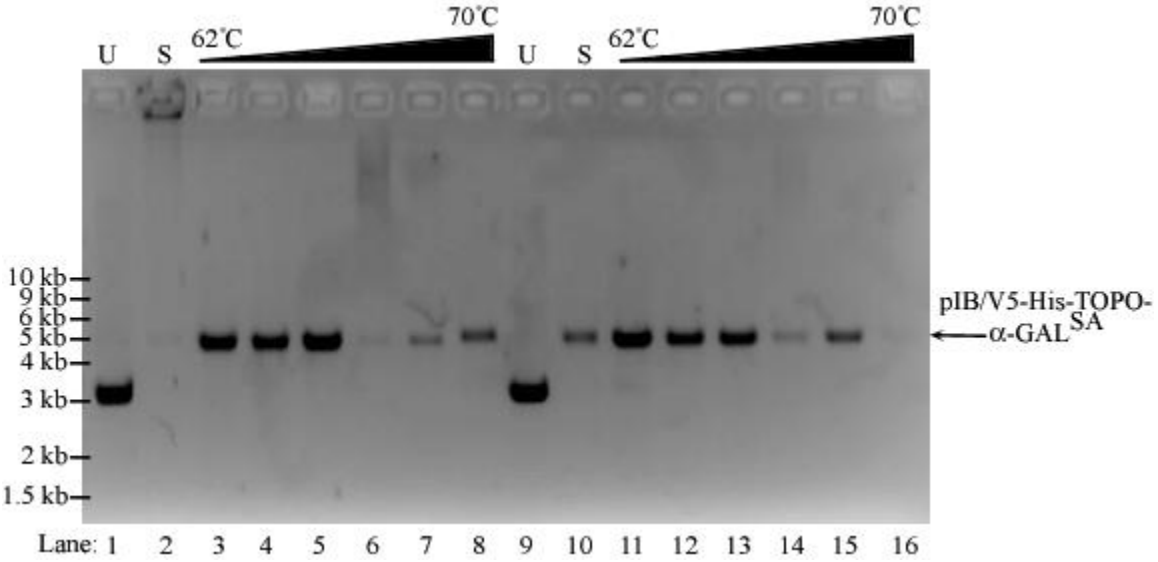

Figure 2: PCR Mutagenesis Gel. PCR mutagenesis products were subjected to 0.75% agarose gel electrophoresis (stained with EtBr). Lanes 1 and 9, "U"= Undigested super-coil, pIB/V5-His-TOPO-α-GAL (control); Lanes 2 and 10, "S"= Single digest, pIB/V5-His-TOPO-α-GAL (linearized by *HindIII* restriction enzyme digestion) (control); Lanes 3-8 and 11-16, PCR mutagenesis products shown at a gradient of annealing temperatures, from 62.0° to 70.0° C respectively. PCR mutagenesis was performed in duplicate experiments, using two identical pIB/V5-His-TOPO-α-GAL template constructs.

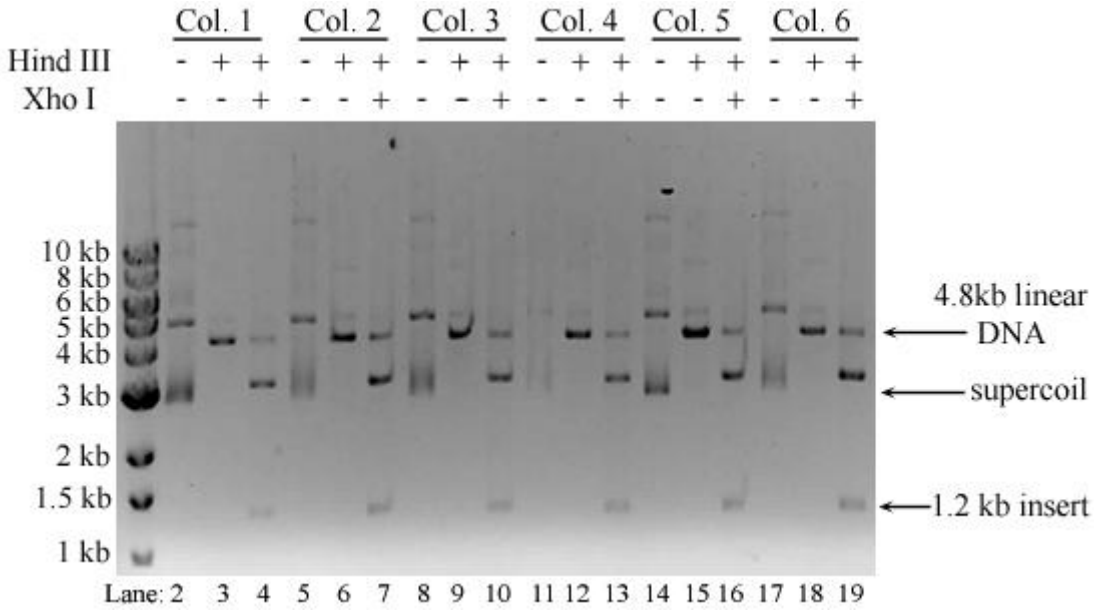

Figure 3: Restriction Digest Gel. The gel shows DNA from *E. coli*. transformed with the α-GAL^{SA} construct. DNA was digested with restriction enzyme, and run on a 0.75% agarose gel (stained with EtBr). Each sample was run undigested (-/-), single-digested (+/-), and double-digested (+/+). Each well is shown loaded with ~12.0 ng of DNA. (Respectively) Lane 1, MW marker (kb); Lanes 2-4, mutant colony 1 uncut, single-digest, double-digest; Lanes 5-7, mutant colony 2 uncut, single-digest, double-digest; Lanes 8-10, mutant colony 3 uncut, single-digest, double-digest; Lanes 11-13, mutant colony 4 uncut, single-digest, double-digest; Lanes 14-16, mutant colony 5 uncut, single-digest, double-digest; Lanes 17-19, mutant plasmid colony 6 uncut, single-digest, double-digest.

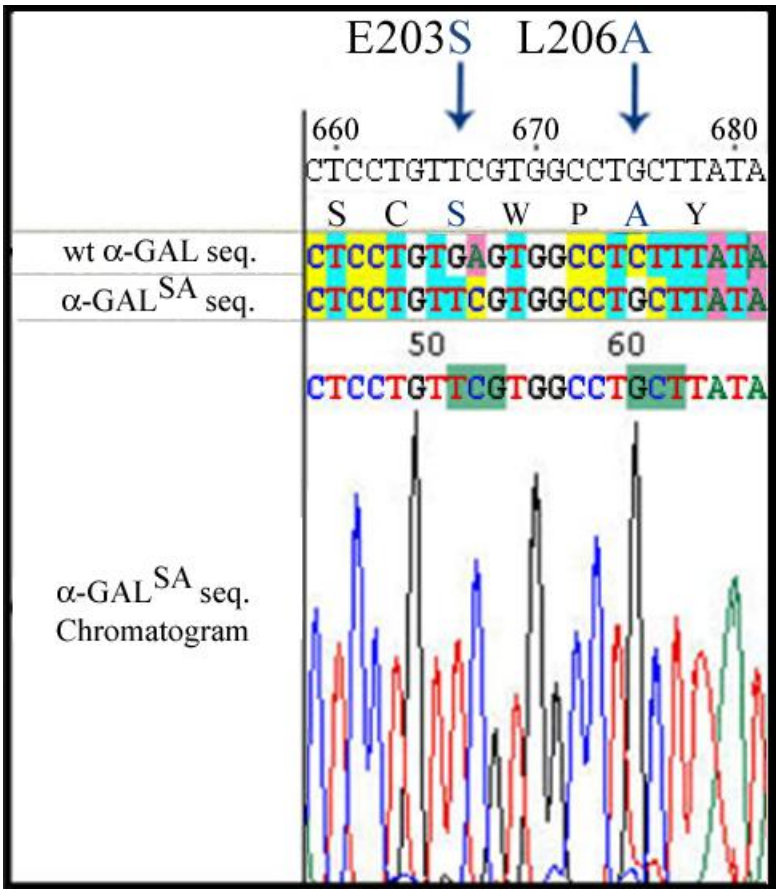

Figure 4: DNA Sequence Chromatogram of α-GAL^{SA}. The α-GAL^{SA} DNA sequence chromatogram was assembled with ChromasPro version 1.41 using sequencing data obtained from GENEWIZ DNA Sequencing Services. Codons containing the E203S, and L206A mutations are highlighted in dark green, and mutant amino acids in the sequence translation are colored blue. The WT α-GAL DNA sequence is shown aligned with α-GAL^{SA}. Mismatched bases between the two sequences show the mutations introduced via PCR mutagenesis.

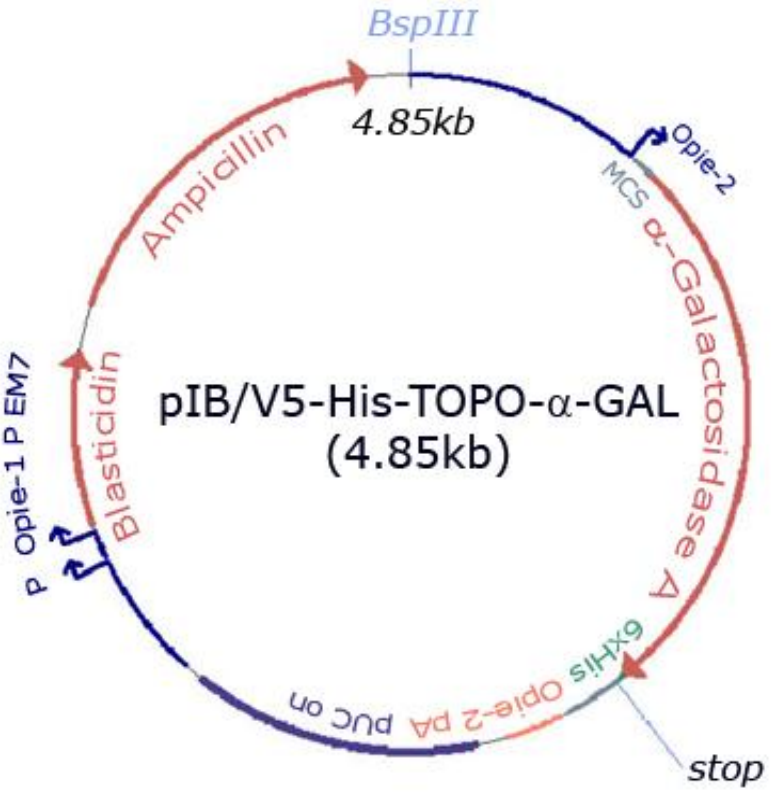

Figure 5: Map of pIB-V5-His-TOPO-α-GAL (4.85 kb). The construct contains *GLA* (Accession code: NM_000169.2), encoding the 429 amino acid α-GAL glycoprotein, and its 31 amino acid signal sequence (~1.2 kb). A 6xHIS tag is linked to the C-terminus of the enzyme. Expression is regulated via the constitutive *OpIE-2* promoter. Blasticidin and ampicillin antibiotic resistance genes are present to facilitate eukaryotic and bacterial selection, respectively.

Figure 6: α-GAL^{SA} Stable Cell Line. (A) A 300 mL suspension culture of the α-GAL^{SA} stable insect cell line, at 27° C. (B) An adherent culture of the α-GAL^{SA} stable insect cell line, at 27° C.

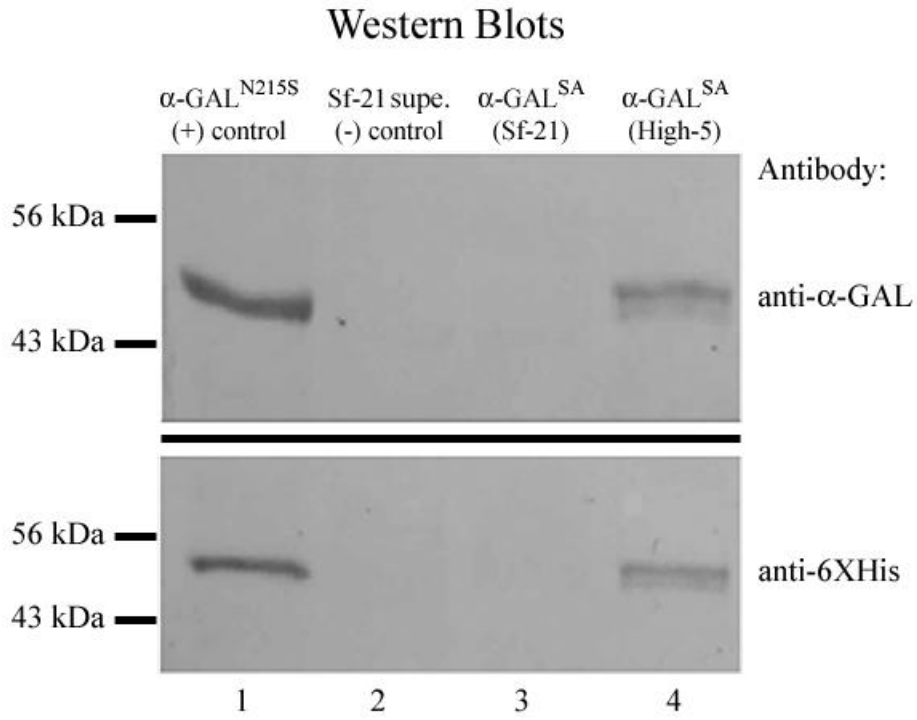

Figure 7: Western Blots of α-GAL^{SA}. Western blots were probed with either monoclonal anti-α-GAL, or polyclonal anti-hexahistidine. Western blots were treated with the appropriate alkaline phosphatase conjugated secondary antibody (anti-chicken, or anti-mouse) and developed with NBT/BCIP substrate. (Both western blots): Lane 1; N215S α-GAL mutant supernatant from High-5 insect cells (positive control); lane 2, Sf21 insect cell supernatant (negative control); lane 3, α-GAL^{SA} supernatant from Sf21 insect cells; lane 4, α-GAL^{SA} supernatant from High-5 insect cells. α-GAL^{SA} expressed at detectable levels in Tn-5 insect cells.

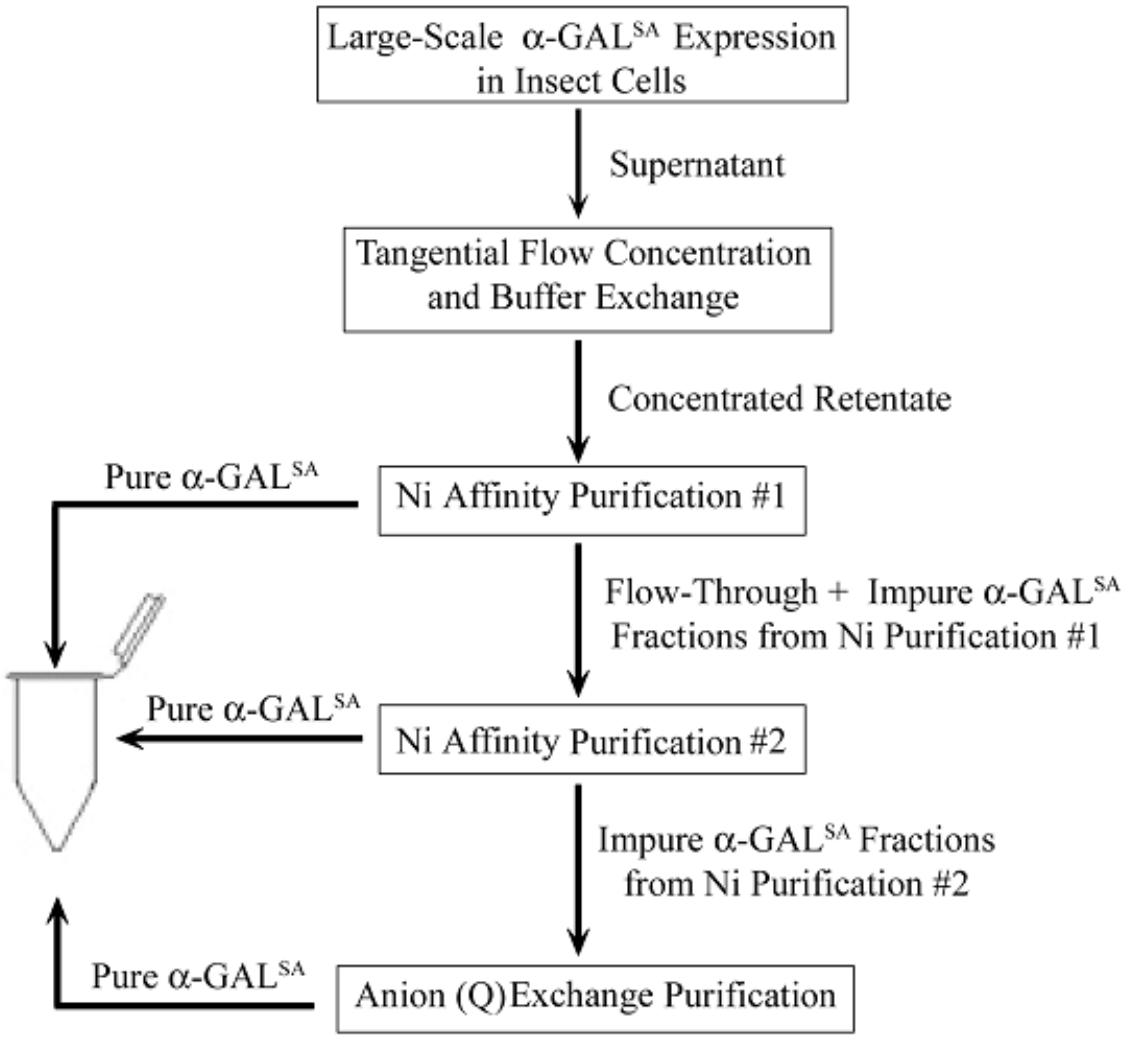

Figure 8: Purification Overview. Flow chart summarizing the purification process used to generate pure α-GAL^{SA} protein, at ~7 mg/mL.

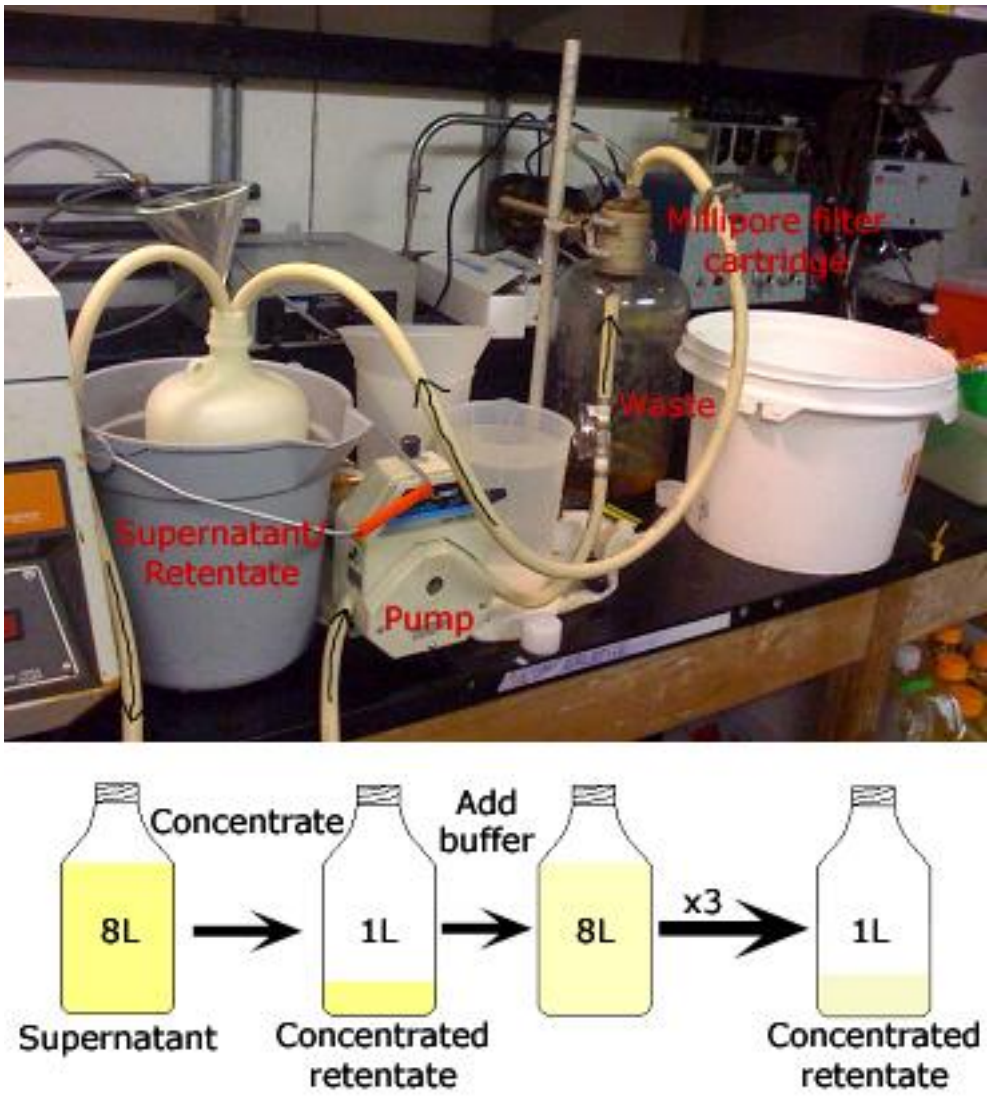

Figure 9: Tangential Flow Setup. (Above): Depiction of the tangential flow (TF) apparatus. Tangential flow filtration is used to concentrate and buffer exchange tissue culture supernatant. Supernatant travels to the pump, then to the Millipore cartridge (MWC 10 kDa), and back to its reservoir/retentate container (arrows). Supernatant that passes through the cartridge membrane is pumped into the waste container. (Cartoon): Simplified representation of the tangential flow process. A large volume of supernatant is pumped through a filter cartridge until ~1 liter of retentate remains. The retentate is diluted and subjected to further TF concentration. The filtration continues until the retentate is clarified.

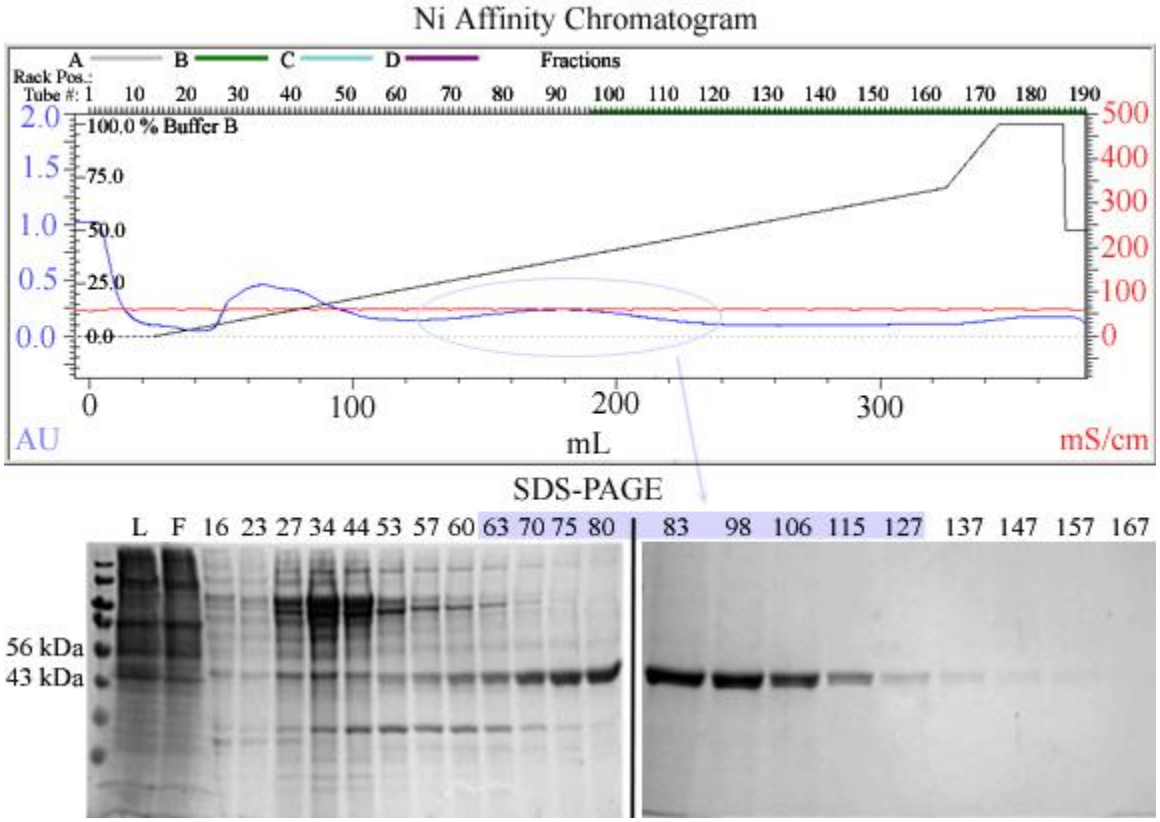

Figure 10: Ni purification # 1. ~ 1 liter of concentrated α-GAL^{SA} retentate was loaded onto a prepacked, 5 ml Ni Sepharose column. A 25ml wash step (Ni Wash Buffer) preceded a 300 ml elution gradient of 0-70% (using Ni Elution Buffer). The UV 280nm absorbance chromatogram is shown in blue. The elution gradient is shown in black. Conductivity is shown in red. The UV 280 nm absorbance peak corresponding to eluted α-GAL^{SA} fractions is circled in purple. Fractions were collected every 2ml, and α-GAL^{SA} was monitored via SDS-PAGE, stained with Coomassie Brilliant Blue. (SDS-Gels): First lane, MW marker; Lane L, load; lane F, flow-through; all remaining lanes, eluted fractions (as labeled). Eluted α-GAL^{SA} appears between the 56 kDa and 43 kDa ladder marker, appearing most prevalent between fractions 63 and 127 (purple).

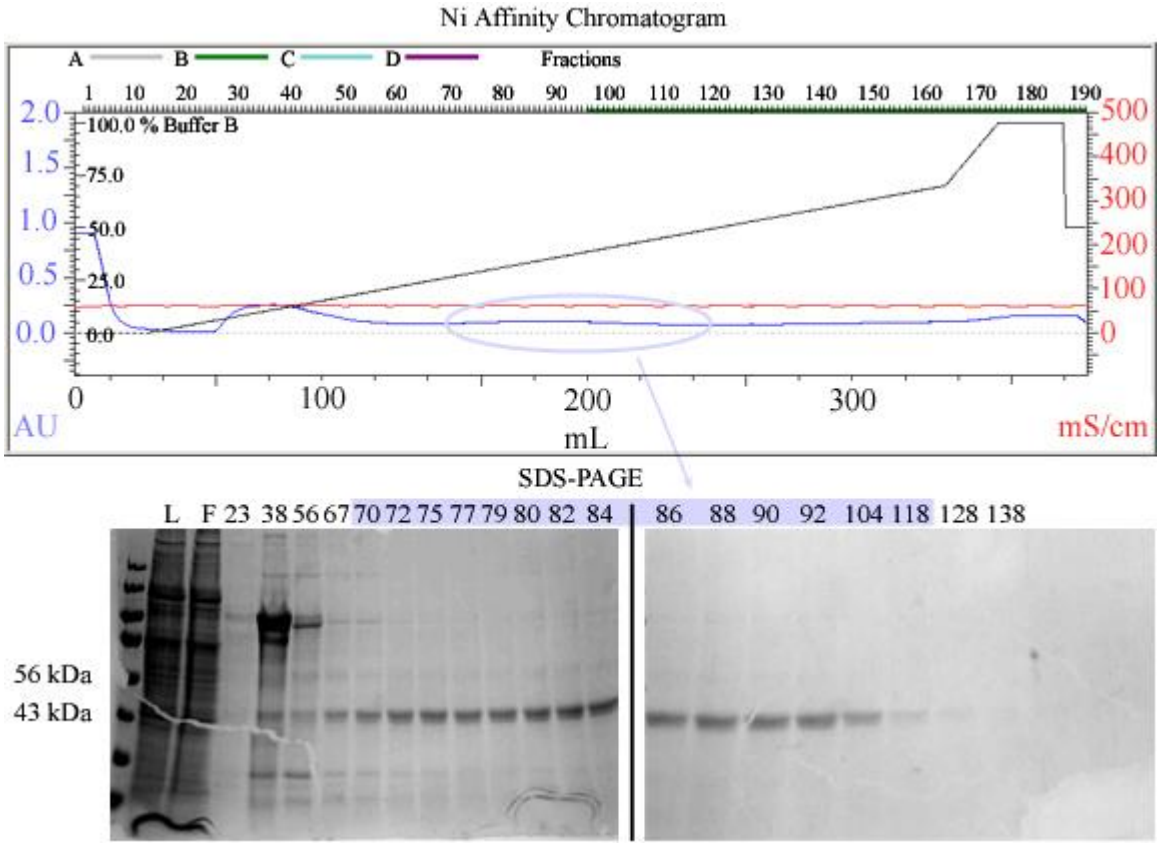

Figure 11: Ni purification # 2. Impure fractions (and the flow-through) from the first Ni affinity chromatography purification were subjected to a second Ni purification. A 25 ml wash step (Ni Wash Buffer) preceded a 300 ml elution gradient of 0-70% (Ni Elution Buffer). The 280 nm absorbance chromatogram is shown in blue. The elution gradient is shown in black. Conductivity is shown in red. The 280 nm absorbance peak corresponding to eluted α-GAL^{SA} is circled in purple. Fractions were collected every 2 ml. α-GAL^{SA} was monitored via SDS-PAGE, stained with Coomassie Brilliant Blue. (SDS-Gels): First lane, MW marker; Lane L, load; lane F, flow-through; all remaining lanes, eluted fractions (as labeled). Eluted α-GAL^{SA} appears between the 56 kDa and 43 kDa ladder marker, appearing most prevalent between fractions 70-118 (purple).

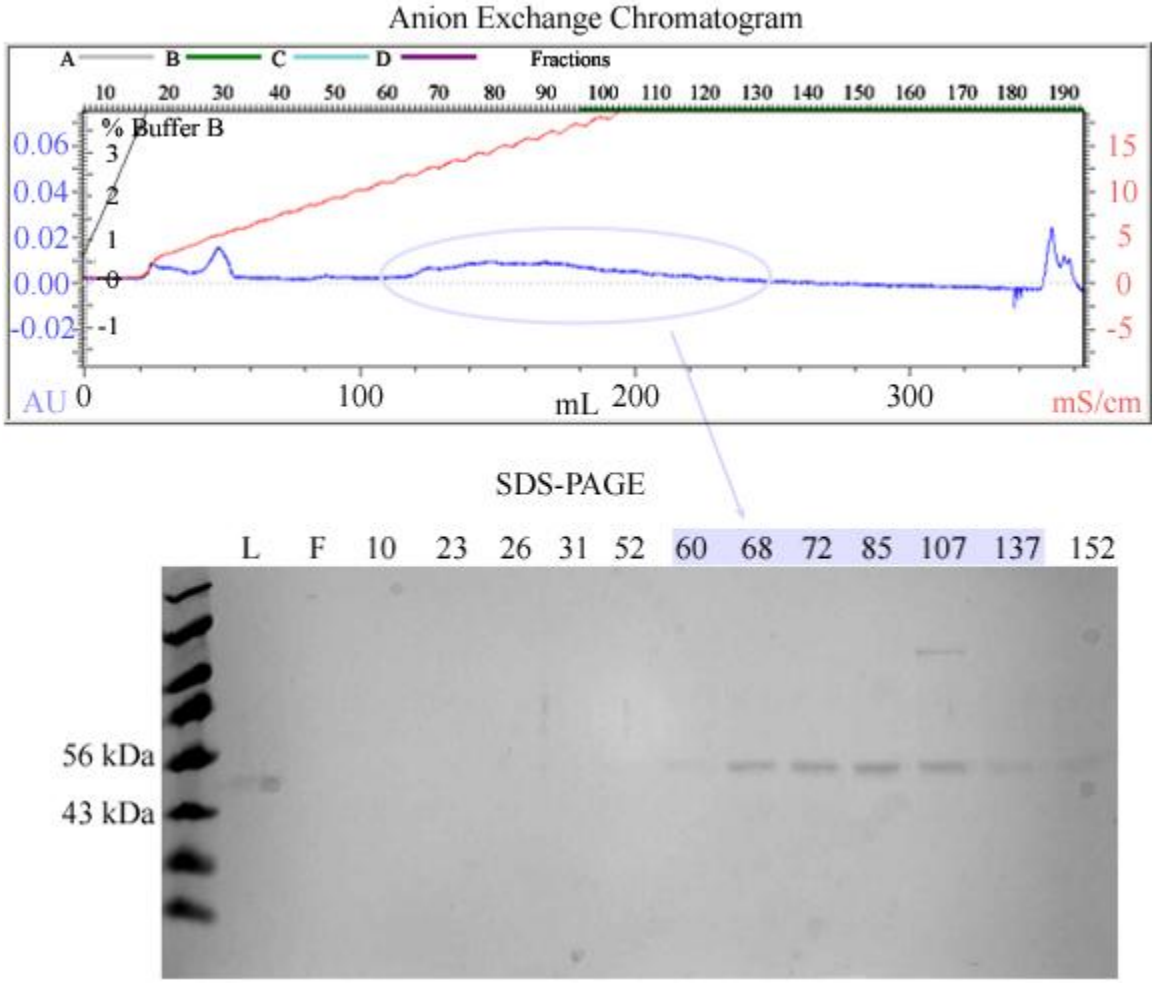

Figure 12: Anion Exchange Chromatography Purification. Further purification of some fractions proceeded by anion (Q) exchange chromatography. Impure α-GAL^{SA} was dialyzed (20 mM Bis-Tris, pH 7.5) overnight, and loaded onto a 1 ml UNO™ Q anion exchange column. An elution gradient of 0-100% (20 mM Bis-Tris, 1 M NaCl, pH 7.5) over a volume of 350 ml was used. The UV 280 nm absorbance chromatogram is shown in blue. The elution gradient is shown in black. Conductivity is shown in red. The 280 nm absorbance peak corresponding to eluted α-GAL^{SA} is circled in purple. Fractions were collected every 2 ml, and α-GAL^{SA} was monitored with SDS-PAGE, stained with Coomassie Brilliant Blue. (SDS Gels): First lane, MW marker; Lane L, load; lane F, flow-through; all remaining lanes, eluted fractions (as labeled). Eluted α-GAL^{SA} appears between the 56 kDa and 43 kDa ladder marker, appearing most prevalent between fractions 60-137 (purple).

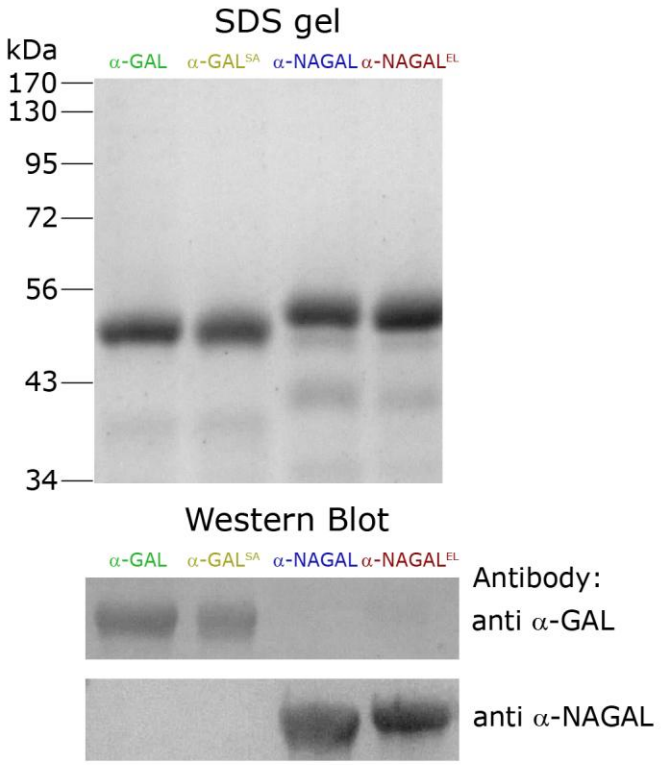

Figure 13: α-GAL^{SA} and α-NAGAL^{EL} Biochemistry. (SDS gel): From left to right, purified α-GAL, α-GAL^{SA}, α-NAGAL, and α-NAGAL^{EL}, stained with Coomassie Brilliant Blue. Both α-GAL and α-GAL^{SA} (3 glycosylation sites) electrophorese to about 50 kDa, while α-NAGAL and α-NAGAL^{EL} both electrophorese to about 52 kDa (5 glycosylation sites). The SDS gel shows that all four proteins are pure, and are at approximately equal concentrations. (Western Blot): From left to right, α-GAL, α-GAL^{SA}, α-NAGAL, and α-NAGAL^{EL}. The two western blots were probed with either monoclonal anti-α-GAL IgG antibody, or polyclonal anti-α-NAGAL IgG antibody. Both blots were treated with the appropriate alkaline phosphatase conjugated secondary antibody and developed with NBT/BCIP substrate. The data show that each mutant protein maintains the antigenicity profile of its corresponding WT parent enzyme. The data also show that cross-reactivity between the mutants or their parent enzymes does not occur.

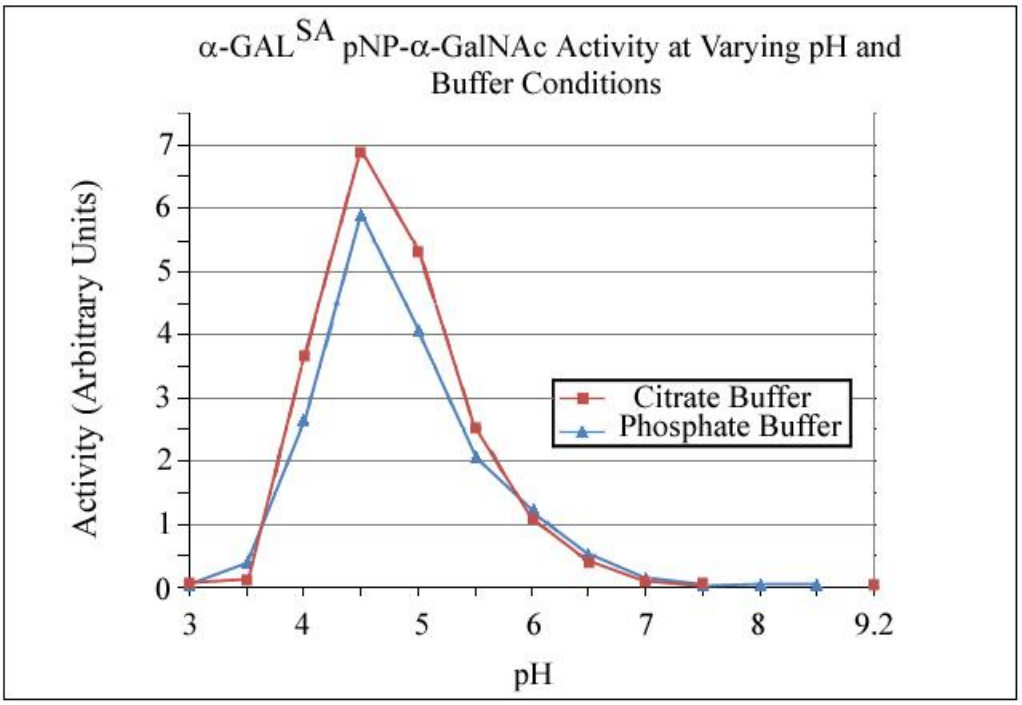

Figure 14: Optimal pH and Buffer for α-GAL^{SA}. A plot of α-GAL^{SA} activity against the synthetic substrate pNP-α-GalNAc, measured between pH 3 to pH 9.2, in either citrate or phosphate buffer. The data show that α-GAL^{SA} activity is highest at pH 4.5, in citrate buffer. The assay was conducted using clear flat bottom 96-well sterile plates, and 400 nm absorbance measurements were taken using a Molecular Devices SpectraMax M5 automated plate reader.

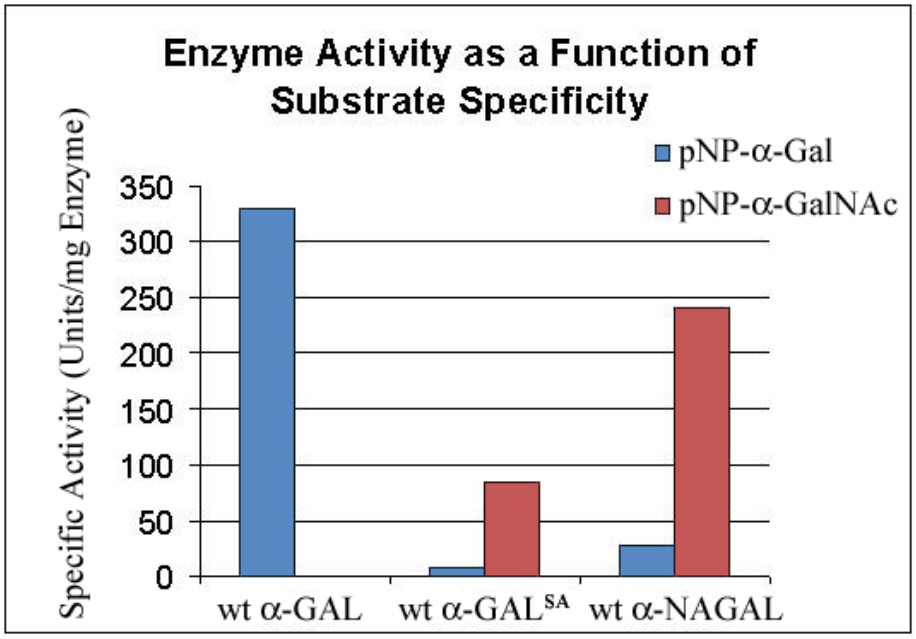

Figure 15: α-GAL^{SA} Specific-Activity. α-GAL^{SA}, α-GAL, and α-NAGAL were subjected to specific-activity assays. The three enzymes were assayed against both pNP-α-Gal, and pNP-α-GalNAc. The data show that α-GAL^{SA} has higher activity against the pNP-α-GalNAc substrate, but that the enzyme is less active than α-NAGAL. Activity was normalized to protein concentration. One Unit releases 1.0 μMole of pNP from pNP-α-Gal or pNP-α-GalNAc per min, at pH 4.5.

Substrate:	pNP-α-Gal			pNP-α-GalNAc		
Enzyme	K_M (mM)	k_{cat} (sec^{-1})	k_{cat} / K_M (mM^{-1} sec^{-1})	K_M (mM)	k_{cat} (sec^{-1})	k_{cat} / K_M (mM^{-1} sec^{-1})
α-GAL	6.88 ± 0.07	37.8 ± 0.2	5.49 ± 0.06	No activity detected *		
α-NAGAL^{EL}	7.58 ± 0.07	13.7 ± 0.1	1.81 ± 0.02	No activity detected *		
α-NAGAL	27.5 ± 4.7	10.7 ± 0.9	0.39 ± 0.07	0.68 ± 0.01	15.1 ± 0.1	22.4 ± 0.1
α-GAL^{SA}	49.1 ± 7.2	1.20 ± 0.14	0.024 ± 0.005	21.0 ± 0.8	21.5 ± 0.7	1.03 ± 0.03

* $k_{cat} < 0.01$ sec^{-1}

Figure 16: Michaelis-Menten Kinetic Data. Michaelis-Menten Kinetic data taken on α-GAL, α-GAL^{SA}, α-NAGAL, and α-NAGAL^{EL} by measuring the amount of pNP cleaved from pNP-α-GAL or pNP-α-GalNAc over time , at varying concentrations.

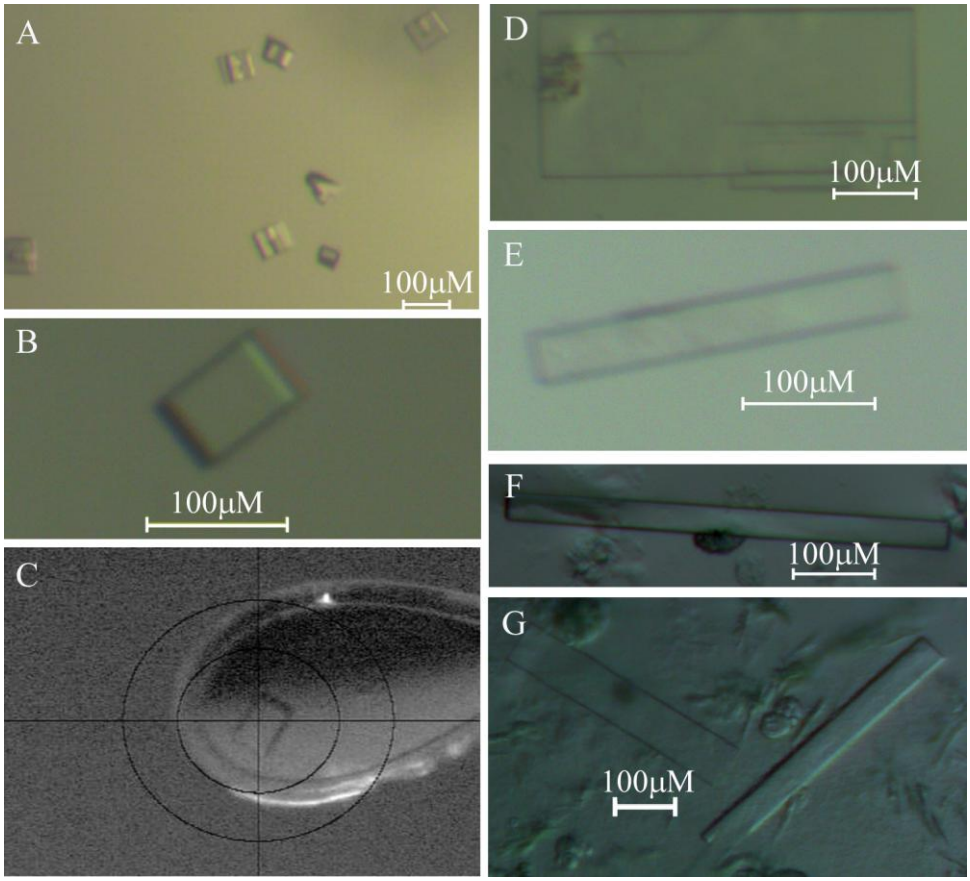

Figure 17: α-GAL^{SA} Crystals. (Image A, B, C): α-GAL^{SA} crystals grown using a reservoir solution of 8% PEG 8 k, 22 mM $Mg(OAc)_2$, 100 mM Sodium Cacodylate, pH 6.5. Crystals from image A were crushed, and used to seed and nucleate the crystals shown in images B and C ($P2_12_12_1$ space group symmetry). The crystal in image C yielded a 3.2 Å dataset. (Images D, E, F, G): α-GAL^{SA} crystals grown using a reservoir solution of 12% PEG 8k, etc,. ($C222_1$ space group symmetry). Image D shows a large crystal demonstrating layered growth with fraying (poor diffraction quality). Crystals of higher diffraction quality are shown in images E, F, and G. These crystals were ligand-soaked with a 200 mM α-GalNAc, or 200 mM α-Gal solution prior to cryo-preservation. The highest resolution dataset diffracted to 2.1 Å.

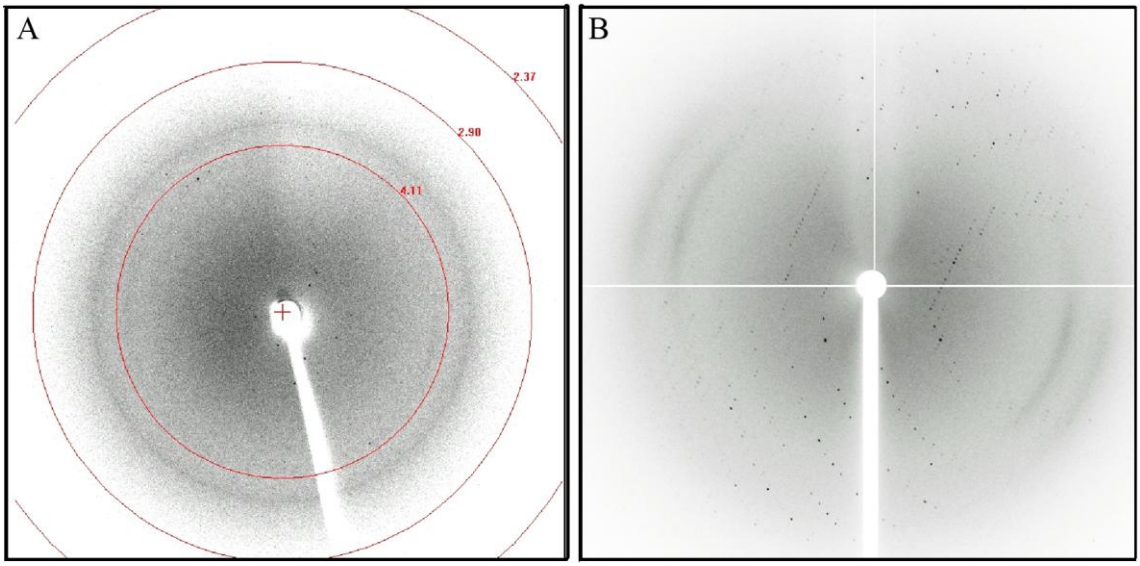

Figure 18 : α-GAL^{SA} Diffraction Images. (A): Five min exposure of the crystal depicted in figure 1.15 (B), using a Rigaku MSC RUH3R X-ray generator (in house), digitally detected using a Raxis IV++ detector. The crystal diffracts to about 3.5 Å, demonstrates non-overlapping spot shape, and has low mosaicity. (B): Diffraction image taken at the X6A beamline at BNL Synchrotron Light Source, with an exposure time of 30 seconds. The more powerful X6A beamline made data collection on such small crystals more feasible than if data were collected in house.

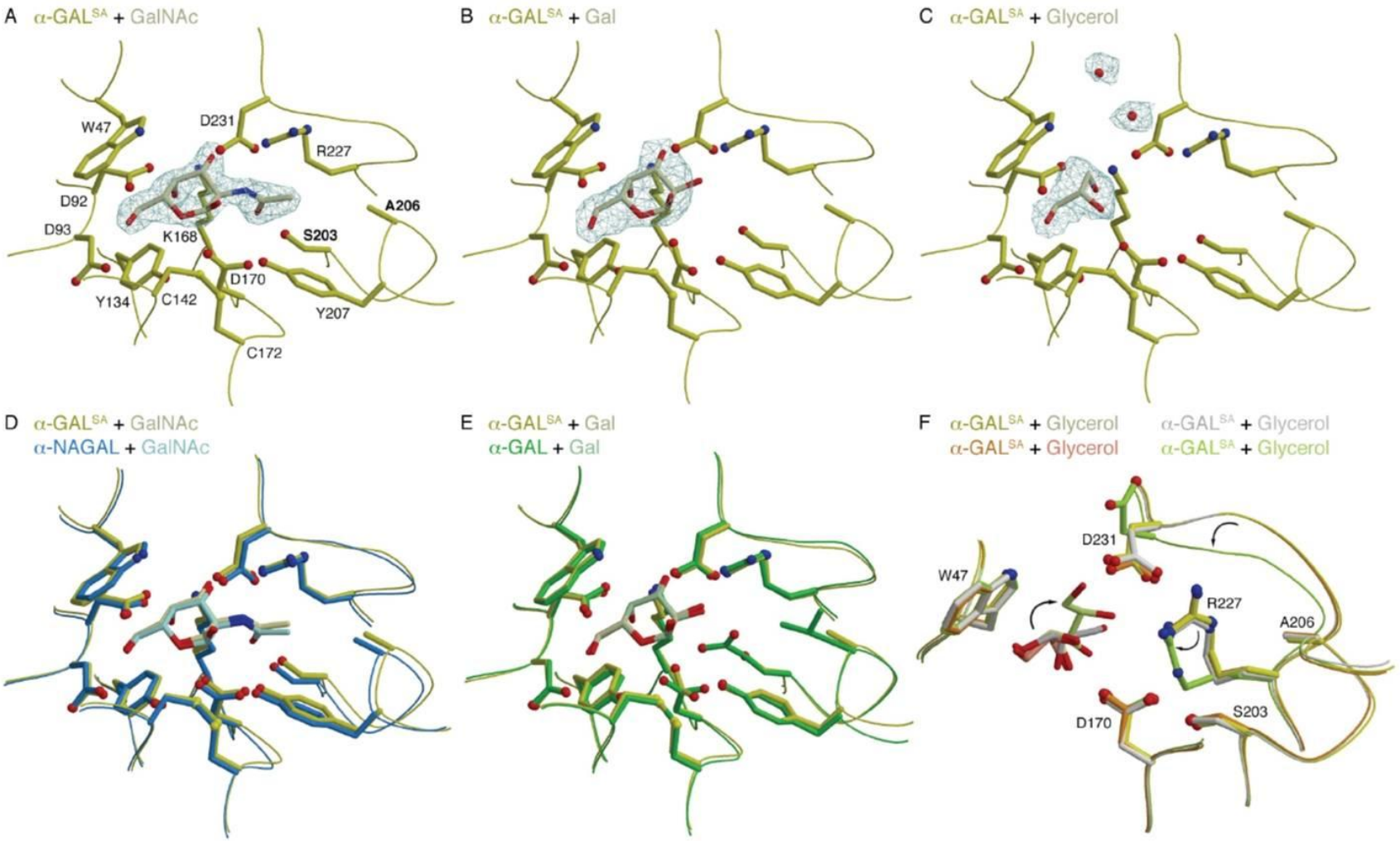

Figure 19: Crystal Structures of α-GAL^{SA}. (A, B, and C): σ_A-weighted $2F_o$-F_c total omit electron density maps of α-GAL^{SA} calculated using SFCHECK. Ligands and water are shown with electron density. (A): α-GAL^{SA} with α-GalNAc soaked into the active site, contoured at 2.0 σ. (B): α-GAL^{SA} with α-Gal soaked into the active site, contoured at 1.8 σ. (C): α-GAL^{SA} with glycerol

soaked into the active site, contoured at 1.0 σ. (D): α-GAL^{SA} superimposed over α-NAGAL by their $(\beta/\alpha)_8$ barrels, with α-GalNAc soaked into the active site. The ligands superimpose with an RMS deviation of 0.38 Å. (E): α-GAL^{SA} superimposed over α-GAL by their $(\beta/\alpha)_8$ barrels, with α-Gal soaked into the active site. The D170 catalytic nucleophile is in a slightly different orientation in the α-GAL^{SA} structure. (F): The four crystallographically independent glycerol-soaked monomers of α-GAL^{SA}. The R227 side chain, and the β6-α6 loop containing the catylitic acid/base D231 shift in one of the four monomers (green, arrows). The glycerol also orients itself differently in one of the monomers.

Table 1: α-GAL^{SA} Data Collection and Refinement Statistics.

Ligand:	GalNAc	Galactose	Glycerol	Glycerol
PDB ID:	3LX9	3LXA	3LXB	3LXC
Data Collection:				
Beamline	APS 24-ID-C	NSLS X6A	NSLS X6A	APS 24-ID-C
Wavelength (Å)	1.07188	0.98010	0.98010	1.07188
Space group	$C222_1$	$P2_12_12_1$	$P2_12_12_1$	$C222_1$
Resolution (Å) (last shell)	50-2.05 (2.09-2.05)	50-3.0 (3.11-3.0)	50-2.85 (2.90-2.85)	50-2.35 (2.39-2.35)
Cell parameters *a*, *b*, *c* (Å)	89.95, 139.49, 182.58	59.50, 105.85, 181.85	59.57, 106.92, 181.51	89.75, 139.77, 182.45
No. of observations	481,042	172,299	136,330	193,566
No. of unique observations (last shell)	72,009 (3,354)	23,638 (2,309)	27,897 (1,334)	47,535 (2,335)
Multiplicity (last shell)	6.7 (3.6)	7.3 (7.2)	4.9 (4.9)	4.1 (4.0)
Completeness (%) (last shell)	99.4 (93.3)	100.0 (99.9)	99.3 (99.9)	98.6 (98.7)
R_{sym} (last shell)	0.120 (0.701)	0.271 (0.851)	0.177 (0.616)	0.153 (0.862)
I/σ_I (last shell)	18.6 (1.6)	7.6 (1.8)	9.1 (2.2)	12.3 (2.0)
Refinement:				
R_{work}/R_{free} , %	17.62/21.82	21.45/24.39	22.50/26.38	18.35/23.68
No. of atoms	7057	6557	6657	7032
Protein	6241	6303	6320	6241
Carbohydrate	257	218	170	227
Water	559	36	131	552
Other	0	0	36	12
Average B, Å^2	37.5	34.5	32.5	45.3
Protein Average B, Å^2	36.3	33.9	31.8	44.4
Ramachandran Plot:				
Favored (%)	91.4	89.5	89.5	89.7
Allowed (%)	8.0	9.6	9.6	9.5
Generous (%)	0.3	0.6	0.9	0.7
Forbidden (%)	0.3	0.3	0.0	0.1
RMS deviations:				
Bonds (Å)	0.0053	0.0150	0.0088	0.0081
Angles (°)	1.056	1.502	1.222	1.172

$R_{sym}=\Sigma_h\Sigma_i|I_{h,i}-\langle I_h\rangle|/\Sigma_h\Sigma_i|I_{h,i}|$, where $I_{h,i}$ is the i^{th} intensity measurement of reflection h and $\langle I_h\rangle$ is the average intensity of that reflection.

R_{work} , $R_{free}=\Sigma_h|F_P-F_C|/\Sigma_h|F_P|$, where F_C is the calculated and F_P is the observed structure factor amplitude of reflection h for the working or free set, respectively.

Ramachandran statistics were calculated in PROCHECK.

APPENDIX A

PROTOCOLS

Phusion PCR Mutagenesis Protocol

Primers should be designed to a length of 24 to 30 nt. The forward primer should contain the desired mismatch mutations near the primer center, flanked on both sides by 10-15 perfectly matched nucleotides. Percent GC content should remain above 50%, and the primer annealing temperatures should fall between 65-72˚ C. T_m should be calculated using the nearest neighbor method. Both primers should be 5′ phosphorylated.

Sample preparation for PCR mutagenesis

Component	[Final]	50µL
H_2O	add to 50µL	35.5µL
5x Phusion HF Buffer	1x	10.0µL
10mM dNTPs	200µM	1.0µL
Primer E203S L206A Forward (new)	0.5µM	1.0µL
Primer E203S L206A Reverse	0.5µM	1.0µL
pIB/V5-His-TOPO-Agal 1	10pg DNA/50µL reaction @ [pIB/V5-His-TOPO-Agal 1] = 10.0pg/µL	1.0µL
Phusion Hot Start DNA Polymerase	0.02U/µL	0.5µL

Thermocycling protocol

Cycling step	Temperature	Time	Number of Cycles
Initial denaturation	98 °C	30s	1
Denaturation	98 °C	10s	30
Annealing	62-70 °C	30s	
Extension	72 °C	140s	
Final extension	72 °C	10mins	1
	4 °C	hold	

Ligation Protocol for Phusion Site-Directed Mutagenesis Kit

1) Take 25 ng of PCR product from the mutagenesis reaction, which usually equals 1-5 µL. Adjust volume to 5 µL with H_2O.

2) Add 5 µL of 2x Quick Ligation Buffer and mix.

3) Add 0.5 µL of Quick T4 DNA Ligase and mix.

4) Centrifuge briefly and incubate at room temperature (25° C) for 5 min.

5) Chill on ice, then transform or store at -20 °C.

6) Do not heat inactivate. Heat inactivation dramatically reduces transformation efficiency.

Transformation Protocol

1) Add 10 µL of the ligation mixture to *E.coli* cells.

2) Mix by swirling and store cells on ice for 30 min.

3) Transfer tubes into a water circulation bath at 42 ° C for 90 seconds. DO NOT SHAKE CELLS!

4) Add transformed cells to 500 µL Lb medium, and incubate for 45 min.

5) Transfer 100 µL of transformed confluent cells to LB agar plates containing Ampicillin.

6) Let the plates stand for 15 min and then incubate at 37 °C for 12-16 hours.

7) Split the plates and repeat incubation.

8) Store cells in the cooler with parafilm.

Minipreps

Please consult Promega SV DNA miniprep kit protocol if interested.

Transfection: Generating Stable Insect Cell Lines

1) Seed a T-25 flask with 3.6 x 10^6 cells, with a viability of 95% or higher (the total

volume in the flask must be at least 4 ml, so you may need to add SFX to dilute the culture).

2) Allow the cells to adhere for twenty min.
3) While the cells are adhering make the transfection mixture (I have found that if you add the DNA to 1.8 ml of SFX, and then add the Cellfectin directly to the mixture, the liposomes form just fine. However, the manufacturer recommends the two mixture protocol described below).

Mixture A	Mixture B
0.9 ml SFX	0.9 ml SFX
.0364 ml Cellfectin	1.8 μg plasmid DNA

4) Mix the two mixtures and gently invert the tube 10 times.
5) Allow the mixture to incubate at room temperature for 15 min (this allows the liposomes to form).
6) Confirm that the cells have adhered to the flask-bottom under the microscope.
7) Remove the SFX from the adhered culture and very slowly add the transfection media to the culture (the mixture should barely cover the culture when rocking).
8) Place the cultures on a rocker, rocking at approximately 2 full rocks / min.
9) Allow the cells to rock for 4 hours.
10) Add 4 ml of SFX to the culture and place the cells in an incubator at 37°C.
11) 48 hours post-transfection remove the SFX/Transfection media from the cells, and replace with fresh SFX with 100 μg/ml blasticidin (you should see blue spheres around some cells).
12) Replace the media with new selective media every two days until the culture

becomes confluent (usually a week and a half).

13) When the selection appears to have been completed replace the media with 5 ml of SFX and suspend the cells.

SDS-PAGE

1) Obtain approximately a 1 ml sample of cell supernatant (supe) and centrifuge at 500 x g for 10 min. Afterwards, remove the supernatant from the pellet and transfer into a clean vial. Avoid disturbing any of the cell pellet at the bottom of the tube.
2) Add 50 µL of supe to 10 µL 6x SDS dye containing 10% 2-mercaptoethanol and boil the samples for 10 min.
3) Make 500 ml of 1x SDS Buffer and fill up the inside of an SDS-PAGE gel box.
4) Load each well of a 10% gel with 15 µL of boiled sample-prep, and 5 µL of protein ladder into lane 1.
5) Run the gel at 200 V for 45 min.

Western Blot

1) Make 1 liter of 1x Transfer Buffer with 20% Methanol.
2) Cut the paper and Nitrocellulose to the appropriate size and soak them in the transfer buffer with the pads.
3) When the SDS-PAGE is complete, assemble the sandwich manifold. Place the negative (black) side down flat. Over the black side place the pads, paper, gel, nitrocellulose membrane, paper, and second pad into the sandwich in that order.
4) Roll out any bubbles and run the sandwich at 100 V for 60 min.

5) After the run, wash the nitrocellulose membrane 2 x in TBS for 10 min.
6) Block with BSA (25 mg/ml) in TBS-T for at least one hour.
7) Wash 2x with TBS and 1x with TBST for 10 min.
8) Incubate with 1° antibody for 1 hour. (1:2000 IgG polyclonal anti-α-Gal in 10 ml TBS-T with BSA)
9) Wash 2x with TBS and 1x with TBS-T for 10 min.
10) Incubate with 2° antibody for 1 hour. (1:5000 anti-chicken in 10ml TBS-T with BSA)
11) Wash 4x with TBS for 10 min.
12) Develop with 2-3 ml of NBT/BCIP substrate.
13) Neutralize AP reaction with water.

α-GAL^{SA} Sample-Prep and Purification Protocol

Ni Wash buffer	Ni Elution Buffer
20 mM Sodium Phosphate	20 mM Sodium Phosphate
500 mM NaCl	500 mM NaCl
20 mM Imidazole, pH 7.5	250 mM Imidazole, pH 7.5

1) Grow desired amount of cells in culture (usually around 10L). When cells reach ~5 x 10^6cells/ml, centrifuge cells and media at 500 x g for 10 min and collect the supernant. Discard the cell pellet, and centrifuge the supernant at max speed for about 1 hour. Again collect the supernant and discard the pellet. The supe should appear very clear.

2) Add 1 ml of 0.05% Azide for every liter of supe.
3) Perform prep/scale tangential flow filtration. When the 10 liters of supe reaches a volume of approximately 1 liter, add 4 liters of Ni Wash Buffer, and continue concentrating. Allow the supe to concentrate to a volume of about 300 ml, and then raise the volume to approximately 1 liter with Ni wash buffer. Repeat until the supe is almost completely clear, with just a slight hint of yellow.
4) Centrifuge the product of tangential flow (retentate) at maximum speed for approximately 1 hour and collect the supernant again. Tangential flow often results in some amount of precipitation.
5) Prepare a pre-packed 5 ml HisTrap FF Ni Sepharose affinity column for Ni affinity chromatography by stripping and recharging the column. Refer to HisTrapFF manual for instruction on how to strip and recharge their pre-packed columns.
6) Pump the load/retentate (isocratic flow) through the column at 2 ml/min for the volume of the given load, and be sure to collect the waste.
7) Now collecting fractions, wash the column with 25ml Ni wash buffer at a rate of 2 ml/min (isocratic flow).
8) Initiate a linear gradient from 0-70% elution buffer over a volume of 300 ml, at a flow rate of 2 ml/min.
9) Raise the elution buffer concentration to 100% for 25 ml, at a flow rate of 2 ml/min.
10) Wash the column with H_20 for 25 ml at a rate of 5 ml/min and store the column in 20% EtOH.

11) Assay fractions via SDS-PAGE, pooling clean fractions for concentration. Set impure fractions aside for an additional Ni purification, and then a final Q-column anion exchange chromatography purification.

Anion Exchange Chromatography Protocol

Q-Wash Buffer	Q-Elution Buffer
20 mM Bis-Tris, pH 7.5	20 mM Bis-Tris
	1.0 M NaCl, pH 7.5

1) Prepare 4 liters of Q-wash buffer for dialysis.
2) Dialyze impure fractions at 4° C with Q-wash buffer. Replace the buffer every 2-3 hours and repeat 3-4 times.
3) Equilibrate the 1.3 ml Q-column as described in the in the Bio-Rad UNO Q Ion Exchange Chromatography Instruction manual.
4) Flow the load through the column at a flow rate of 1 ml/min, collecting the flow-through.
5) Wash the column with 10 mL of Q-wash buffer at a flow rate of 1ml/min, now collecting fractions (isocratic flow).
6) Establish a linear gradient of 0-100% Q-elution buffer over a volume of 300 ml, at a flow rate of 1 ml/min while collecting fractions.
7) Wash the column with 10 ml of Q-elution buffer (isocratic flow) at a flow rate of 1 ml/min, collecting fractions.
8) Store the column in 20% EtOH.
9) Perform SDS-PAGE on fractions and pool clean fractions for concentration.

Protein Concentration

1) Use Sartorius Biolab Products Vivaspin 6 concentrator with a MWC of 10 kDa. Refill the concentrators with pooled fractions until all have flowed through the concentrator and are at a volume of ~1 ml. Centrifuge at a max of 4000 x g.
2) Buffer exchange with 10 mM Sodium Phosphate buffer pH 6.5, and repeat 3 times.
3) When a final volume of about 500 μL is reached, attain 280 nm absorbance measurements via spectrophotometer and calculate protein concentration.

***para*-Nitrophenol-linked Specific-Activity**

Reagents:

A) 100 mM Citrate and 100 mM Sodium Phosphate Buffer, pH 4.5. Adjust pH with 1 M NaOH or 1 M HCl.
B) 100 mM Citrate and 100 mM Sodium Phosphate Buffer, pH 4.5 with 0.1% Bovine Serum Albumin. (Enzyme diluent)
C) 5.0 mM *para*-Nitrophenol N-acetyl-α-D-galactosaminide (pNP-α-GalNAc) or p-Nitrophenol α-D-galactopyranoside (pNP-α-Gal). Prepare with reagent A.
D) 200 mM Borate Buffer, pH 9.8. Adjust pH with 1 M NaOH.
E) Enzyme solution. Prepare α-NAGAL or α-GAL dilutions in reagent B.

Procedure: Pipette in μL the fallowing reagents into suitable containers:

	Test	Blank
Reagent C, (PNP-α-GalNAc or PNP-α-Gal)	10 μL	10 μL

Equilibrate to 37°C. Then add:

Reagent E (Enzyme solution)	5 μL	---------

Immediately mix and incubate at 37°C for exactly 10 min. Then add:

Reagent D (Borate)	100 μL	100 μL
Reagent E (Enzyme solution)	---------	5 μL

Mix and transfer to suitable cuvettes. Record Absorbance 400nm for both test and blank using a spectrophotometer.

Calculations:

$$\text{Units / ml Enzyme} = \frac{(\text{Abs 400 nm Test} - \text{Abs 400 nm Blank})\ (V)\ (df)}{(18)\ (10)\ (0.005)} \quad (1)$$

Where:

0.115 = Total volume (in ml) of assay.

df = Dilution factor.

18 = Millimolar extinction coefficient of p-Nitrophenolate at 400 nm

10 = time (in min) of assay per the Unit Definition.

0.005 = Volume (in ml) of enzyme used.

$$\text{Units / mg solid} = \frac{\text{Units / ml enzyme}}{\text{Mg solid / mg enzyme}}$$

$$\text{Units / mg protein} = \frac{\text{Units / ml of enzyme}}{\text{Mg protein / ml of enzyme}}$$

Unit Definition: One Unit will release 1.0 μmole of *para*-Nitrophenol from p-Nitrophenol-α-D-galactosaminide (pNP-α-GalNAc) or *para*-Nitrophenol α-D-galactopyranoside (pNP-α-Gal), per min at pH 4.5, 37° C.

APPENDIX B

SEQUENCES

Human α-Galactosidase A sequence

```
 1   aaacaataac gtcattattt aataagtcat cggtgattgg tccgcccctg aggttaatct

61   taaaagccca ggttacccgc ggaaatttat gctgtccggt caccgtgaca atgcagctga
                                                          M   Q   L   R

121  ggaacccaga actacatctg ggctgcgcgc ttgcgcttcg cttcctggcc ctcgtttcct
       N   P   E   L   H   L   G   C   A   L   A   L   R   F   L   A   L   V   S   W

181  gggacatccc tggggctaga gcactggaca atggattggc aaggacgcct accatgggct
       D   I   P   G   A   R   A  L   D   N   G   L   A   R   T   P   T   M   G  W44

241  ggctgcactg ggagcgcttc atgtgcaacc ttgactgcca ggaagagcca gattcctgca
       L   H   W   E   R   F   M   C   N   L   D   C   Q   E   E   P   D   S   C  I64

301  tcagtgagaa gctcttcatg gagatggcag agctcatggt ctcagaaggc tggaaggatg
       S   E   K   L   F   M   E   M   A   E   L   M   V   S   E   G   W   K   D  A84

361  caggttatga gtacctctgc attgatgact gttggatggc tccccaaaga gattcagaag
       G   Y   E   Y   L   C   I   D   D   C   W   M   A   P   Q   R   D   S   E  G104

421  gcagacttca ggcagaccct cagcgctttc ctcatgggat tcgccagcta gctaattatg
       R   L   Q   A   D   P   Q   R   F   P   H   G   I   R   Q   L   A   N   Y  V124

481  ttcacagcaa aggactgaag ctagggattt atgcagatgt tggaaataaa acctgcgcag
       H   S   K   G   L   K   L   G   I   Y   A   D   V   G   N   K   T   C   A  G144

541  gcttccctgg gagttttgga tactacgaca ttgatgccca gacctttgct gactggggag
       F   P   G   S   F   G   Y   Y   D   I   D   A   Q   T   F   A   D   W   G  V164

601  tagatctgct aaaatttgat ggttgttact gtgacagttt ggaaaatttg gcagatggtt
       D   L   L   K   F   D   G   C   Y   C   D   S   L   E   N   L   A   D   G  Y184

661  ataagcacat gtccttggcc ctgaatagga ctggcagaag cattgtgtac tcctgtgagt
       K   H   M   S   L   A   L   N   R   T   G   R   S   I   V   Y   S   C   E  W204

721  ggcctcttta tatgtggccc tttcaaaagc ccaattatac agaaatccga cagtactgca
       P   L   Y   M   W   P   F   Q   K   P   N   Y   T   E   I   R   Q   Y   C  N224

781  atcactggcg aaattttgct gacattgatg attcctggaa aagtataaag agtatcttgg
       H   W   R   N   F   A   D   I   D   D   S   W   K   S   I   K   S   I   L  D244

841  actggacatc ttttaaccag gagagaattg ttgatgttgc tggaccaggg ggttggaatg
       W   T   S   E   N   Q   E   R   I   V   D   V   A   G   P   G   G   W   N  D264

901  acccagatat gttagtgatt ggcaactttg gcctcagctg gaatcagcaa gtaactcaga
       P   D   M   L   V   I   G   N   F   G   L   S   W   N   Q   Q   V   T   Q  M284
```

```
961  tggccctctg ggctatcatg gctgctcctt tattcatgtc taatgacctc cgacacatca
       A  L  W  A  I  M  A  A  P  L  F  M  S  N  D  L  R  H  I  S304

1021 gccctcaagc caaagctctc cttcaggata aggacgtaat tgccatcaat caggacccct
       P  Q  A  K  A  L  L  Q  D  K  D  V  I  A  I  N  Q  D  P  L324

1081 tgggcaagca agggtaccag cttagacagg gagacaactt tgaagtgtgg gaacgacctc
       G  K  Q  G  Y  Q  L  R  Q  G  D  N  F  E  V  W  E  R  P  L344

1141 tctcaggctt agcctgggct gtagctatga taaaccggca ggagattggt ggacctcgct
       S  G  L  A  W  A  V  A  M  I  N  R  Q  E  I  G  G  P  R  S364

1201 cttataccat cgcagttgct tccctgggta aaggagtggc ctgtaatcct gcctgcttca
       Y  T  I  A  V  A  S  L  G  K  G  V  A  C  N  P  A  C  F  I384

1261 tcacacagct cctccctgtg aaaaggaagc tagggttcta tgaatggact tcaaggttaa
       T  Q  L  L  P  V  K  R  K  L  G  F  Y  E  W  T  S  R  L  R404

1321 gaagtcacat aaatcccaca ggcactgttt tgcttcagct agaaaataca atgcagatgt
       S  H  I  N  P  T  G  T  V  L  L  Q  L  E  N  Y  M  Q  M  S424

1381 cattaaaaga cttactttaa aatgtttatt ttattgcc
       L  K  D  L  L  STOP
```

Human α-GAL Active Site Amino Acid Residues

W47, D92, D93, Y134, C142, K168, D170, C172, E203, L206, Y207, R227, D231

Human α-NAGAL Active Site Amino Acid Residues

W33, D78, D79, Y119, C127, K154, D156, C158, S188, A191, Y192, R213, D217

APPENDIX C

TOMASIC, I.B., METCALF, M.C., GUCE, A.I., CLARK, N.E., GARMAN, S.C. (MAY 5, 2010) "INTERCONVERSION OF THE SPECIFICITIES OF HUMAN LYSOSOMAL ENZYMES ASSOCIATED WITH FABRY AND SCHINDLER DISEASES." *JBC*, PMID 20444686

Interconversion of the specificities of human lysosomal enzymes associated with Fabry and Schindler diseases

Ivan B. Tomasic[1,3], Matthew C. Metcalf[1,3], Abigail I. Guce[2], Nathaniel E. Clark[1], and Scott C. Garman[1,2]

Departments of Biochemistry & Molecular Biology[1] and Chemistry[2], University of Massachusetts, Amherst MA 01003, USA;
[3]These authors contributed equally to this work

Running Head: Interconversion of enzyme specificities

Address correspondence to: Scott C. Garman, PhD, Dept of Biochemistry & Molecular Biology, 710 North Pleasant Street, University of Massachusetts, Amherst MA 01003. Fax 413-545-3291; E-mail: garman@biochem.umass.edu

The human lysosomal enzymes α-galactosidase (α-GAL, E.C. 3.2.1.22) and α-N-acetylgalactosaminidase (α-NAGAL, E.C. 3.2.1.49) share 46% amino-acid sequence identity and have similar folds. The active sites of the two enzymes share 11 of 13 amino acids, differing only where they interact with the 2- position of the substrates. Using a rational protein engineering approach, we interconverted the enzymatic specificity of α-GAL and α-NAGAL. The engineered α-GAL (which we call α-GAL^{SA}) retains the antigenicity of α-GAL but has acquired the enzymatic specificity of α-NAGAL. Conversely, the engineered α-NAGAL (which we call α-NAGAL^{EL}) retains the antigenicity of α-NAGAL but has acquired the enzymatic specificity of the α-GAL enzyme. Comparison of the crystal structures of the designed enzyme α-GAL^{SA} to the wild type enzymes shows that active sites of α-GAL^{SA} and α-NAGAL superimpose well, indicating success of the rational design. The designed enzymes might be useful as non-immunogenic alternatives in enzyme replacement therapy for treatment of lysosomal storage disorders such as Fabry disease.

Introduction

Lysosomal enzymes are responsible for the catabolism of metabolic products in the cell. Deficiencies in lysosomal enzymes lead to lysosomal storage diseases, characterized by an accumulation of undegraded substrates in the lysosome. In humans, there are at least 40 different lysosomal storage diseases (including, for example, Tay-Sachs, Sandhoff, Gaucher, and Fabry diseases), each of which is caused by a lack of a specific enzymatic activity. Fabry disease is caused by a defect in the *GLA* gene, leading to loss of activity in the enzyme alpha-galactosidase (α-GAL, E.C. 3.2.1.22, also known as α-GAL A)(1). The α-GAL enzyme cleaves substrates containing

terminal α-galactosides, including glycoprotein, glycolipids, and polysaccharides. Defects in the *GLA* gene in Fabry patients lead to the accumulation of unprocessed neutral substrates (primarily globotriaosylceramide, Gb3), which then leads to the progressive deterioration of multiple organ systems and premature death. Fabry disease is an X-linked inherited disorder with an estimated prevalence of approximately 1 in 40,000 male births but may be highly underdiagnosed (1,2).

The human gene most closely related to the *GLA* gene is the *NAGA* gene, encoding the enzyme α-N-acetylgalactosaminidase (α-NAGAL, E.C. 3.2.1.49, also known as NAGA and α-GAL B)(3). The two genes are derived from a common ancestor (4), encoding proteins that share 46% amino-acid sequence identity (Fig. 1A); they belong to glycoside hydrolase family 27 and clan D (5). The α-NAGAL enzyme recognizes and cleaves substrates containing terminal α-N-acetylgalactosaminide (α-GalNAc) sugars, and (less efficiently) substrates containing terminal α-galactosides. Defects in the *NAGA* gene lead to the lysosomal storage disease Schindler disease, characterized by the accumulation of glycolipids and glycopeptides, resulting in a wide range of symptoms, including neurological, skin, and cardiac anomalies (3).

The only approved therapy for the treatment of Fabry disease is enzyme replacement therapy, where patients are injected with recombinant enzyme purified from mammalian cell expression systems (6,7). One problem with this treatment is that up to 88% of patients develop IgG antibodies against the injected recombinant enzyme (6,8). In patients who make no functional α-GAL enzyme, the recombinant α-GAL used in enzyme replacement therapy can be treated as a foreign antigen. Since the *GLA* gene is located on the X-chromosome, hemizygous males who inherit a non-functional copy of the gene have no second copy to establish immunotolerance.

Previously, we determined the three-dimensional crystallographic structures of the human α-GAL and α-NAGAL enzymes (9,10). As expected for two structures that share 46% sequence identity, the overall folds of the two enzymes are similar (Fig. 1B & C). Each enzyme is a dimer where each monomer contains an N-terminal $(\beta/\alpha)_8$ barrel with the active site and a C-terminal antiparallel β domain. The monomers of the two enzymes superimpose with an RMS deviation of 0.90Å for 378 alpha carbons. The active sites of the two structures are highly similar, as 11 of the 13 active site residues are conserved. The only differences in the active sites of the two structures correspond to where the substrates are different: in α-GAL, the residues near the 2-OH on the substrate include larger glutamate and leucine, whereas in α-NAGAL, the larger 2-N-acetyl on the substrate interacts with the smaller serine and alanine residues on the enzyme (Fig. 1B & C). As we and others have noted, in glycoside hydrolase family 27, the two residues primarily responsible for recognition of the 2 position of the ligand are both located on the same loop in the structure, the β5-α5 loop in the $(\beta/\alpha)_8$ barrel domain (9-13).

The similarities between the active sites of the enzymes in the family and the proximity of the two residues responsible for the recognition of the 2 position of the ligand led us and others to hypothesize that interconversion of the enzyme specificities would be possible (9,14). We replaced two residues in the active site of α-GAL (E203S and L206A), leading to a new protein (α-GAL^{SA}) with the enzymatic specificity of an α-NAGAL enzyme. Additionally, we replaced two residues in the active site of α-NAGAL (S188E and A191L), leading to a new protein (α-NAGAL^{EL}) with the enzymatic specificity of an α-GAL enzyme. In this report, we show that the designed enzymes maintain the antigenicity of the original protein, but have the specificity of the other enzyme. X-ray crystallographic studies of the α-GAL^{SA} protein provide a structural basis for ligand specificity in the family of proteins.

Experimental Procedures

Molecular biology: Human α-GAL and human α-NAGAL were expressed in stably transfected *Trichoplusia ni* (Tn5) insect cells as described (10,15). The α-GAL^{SA} variant

was generated from the wild type α-GAL construct using PCR-based site-directed mutagenesis (forward primer 5'-G TAC TCC TGT **TC**G TGG CCT **GC**T TAT ATG TGG-3' [substitutions in bold] and reverse primer 5'-CAC AAT GCT TCT GCC AGT CCT ATT CAG GGC-3'), ligated, transformed into bacteria, and confirmed by sequencing. The α-NAGAL^{EL} variant was derived from the wild type α-NAGAL construct by PCR (forward primer 5'-CGG CCT CCC CCC AAG GGT GAA CTA-3' and reverse primer 5'-CC TTC ATA G**AG** TGG CCA **CTC** GCA GGA GAA-3'), ligated, transformed into bacteria, and sequenced.

Cell transfection: Adherent Tn5 cells in SFX media were transfected with plasmid DNA, and selection for stably transfected cells using 100 μg/mL blasticidin (added after 48 hours and every 48 hours for 10 days). Stable adherent cells were re-suspended in SFX media for larger scale suspension cultures.

Protein expression and purification: 1L cultures of stable cells secreting α-GAL^{SA} and α-NAGAL^{EL} proteins were grown to 3 x 10^6 cells/ml. The supernatant was clarified and concentrated by tangential flow filtration (Millipore Prep/Scale) and exchanged into Ni^{2+} binding buffer (50mM Na_3PO_4, pH 7.0, 250mM NaCl, 20mM imidazole, and 0.01% NaN_3). The filtrate was loaded onto a Ni^{2+}-Sepharose 6 Fast Flow column (GE Healthcare) and eluted with a gradient of 0-60% elution buffer (50mM Na_3PO_4, pH 7.0, 250mM NaCl, 250mM imidazole, and 0.01% NaN_3). Eluate fractions were pooled, desalted, and concentrated before loading onto a Source 15Q anion exchange column. Fractions eluted by a linear salt gradient were screened by activity assays and by western blots. Fractions containing pure protein were pooled and concentrated to 1.0 mg/mL for storage.

Kinetic assays: Hydrolysis of the synthetic substrates *para*-nitrophenyl-α-galactose (pNP-α-Gal) and *para*-nitrophenyl-α-N-acetylgalactosamine (pNP-α-GalNAc) (Toronto Research Chemicals) at 37°C were monitored by absorbance at 400nm using an extinction coefficient of 18.1 mM^{-1} cm^{-1}. 0.25-1.2ug of enzyme in 100mM citrate/phosphate buffer pH 4.5 was added to 12 substrate concentrations (pNP-α-Gal from 0.1 to 50mM, and pNP-α-GalNAc from 0.01 to 10mM). Each minute for 10 minutes, the sample absorbance was measured after adding 200mM Na_3BO_3 buffer, pH 9.8. Error bars were determined from triplicate measurements by two experimenters for each data point. K_M, V_{max}, and k_{cat} and error bars were determined from a weighted fit of Michaelis-Menten hyperbola in KaleidaGraph. Substrate solubility limits prevented saturation in some experiments. Substrate specificity ratios for each enzyme were defined as $(k_{cat}/K_M)_{pNP\text{-}\alpha\text{-}GalNAc}$ / $(k_{cat}/K_M)_{pNP\text{-}\alpha\text{-}Gal}$, indicating the preference of an enzyme for galactosaminide substrates.

Crystallization and X-ray data collection: Crystals of α-GAL^{SA} were grown as described for the D170A α-GAL variant (15). Crystals were obtained from a 1:1 mixture of reservoir solution [12% PEG 8K, 0.1M Na cacodylate pH 6.5, and 22mM $Mg(CH_3COO)_2$] and 7.0 mg/mL protein in 10mM Na_3PO_4, pH 6.5. Crystals were transferred stepwise into reservoir solution containing 200mM ligand (GalNAc or galactose) and then into cryoprotectant solution (15% PEG 8K, 0.1M Na cacodylate pH 6.5, 22mM $Mg(CH_3COO)_2$, 20% glycerol, and 200mM ligand). Crystals were flash cooled in liquid nitrogen and X-ray data were collected at 100K at beamline X6A at the Brookhaven National Laboratory or at the microfocus beamline NECAT 24-ID-C at Argonne National Laboratory. X-ray images were processed using HKL2000 (16) and phased by molecular replacement in AMoRe (17) or by Fourier synthesis using human α-GAL coordinates (PDB: 3HG3) (15). We selected the overall resolution limits based upon I/σ_I criteria. Atomic models were built using the program O (18), with refinement in REFMAC5 (17). Ramachandran plots were computed using PROCHECK (19). Coordinates were superimposed using LSQMAN (20). Figures were made in MolScript (21) and POVScript+ (22). Coordinates and structure factors are deposited in the Protein Data Bank under accession codes 3LX9, 3LXA, 3LXB, and 3LXC.

Results

Biochemical Characterization

We expressed the four enzymes (α-GAL, α-GAL^{SA}, α-NAGAL, and α-NAGAL^{EL}) in stably transfected Tn5 insect cells and purified protein from the supernatant. SDS-PAGE analysis shows that the purified variant proteins migrate at the same size as their wild-type equivalents, approximately 50kDa for α-GAL and α-GAL^{SA} and 52kDa for α-NAGAL and α-NAGAL^{EL} (Fig 1D). To test the antigenicity of the wild type and variant proteins, we performed western blots on all four proteins using antibodies against human α-GAL and human α-NAGAL. α-GAL and α-GAL^{SA} cross-react only with the anti α-GAL antibody, while α-NAGAL and α-NAGAL^{EL} cross-react only with the anti α-NAGAL antibody (Fig 1E), indicating that the variant proteins retain their original antigenicity.

Enzymatic Activity

We tested the four enzymes against two synthetic substrates, *para*-nitrophenyl-α-galactose (pNP-α-Gal) and *para*-nitrophenyl-α-N-acetylgalactosamine (pNP-α-GalNAc). In the wild type enzymes, the larger active site of α-NAGAL allows it to bind and cleave both substrates, although less efficiently against pNP-α-Gal. The smaller active site of α-GAL allows for efficient catalysis of pNP-α-Gal, but no detectable activity on pNP-α-GalNAc due to steric clashes between the N-acetyl group on the 2-position of the sugar and the larger E203 and L206 side chains of α-GAL. Table 1 summarizes the enzyme kinetic data.

The variant enzymes α-GAL^{SA} and α-NAGAL^{EL} show the opposite substrate specificity compared to their starting wild type enzymes. The α-NAGAL^{EL} enzyme shows the catalytic properties of wild type α-GAL: it has no activity against the pNP-α-GalNAc substrate, but shows high activity against pNP-α-Gal. The α-GAL^{SA} enzyme has the catalytic properties of wild type α-NAGAL: it has high activity against pNP-α-GalNAc and reduced activity against pNP-α-Gal.

Since the enzymes in this family have overlapping substrate specificity, we used the ratio of the specificity constant k_{cat}/K_M for the two substrates as a measure of the enzymes' ability to discriminate between the two related substrates. The substrate specificity ratios $(k_{cat}/K_M)_{pNP\text{-}\alpha\text{-}GalNAc}$ / $(k_{cat}/K_M)_{pNP\text{-}\alpha\text{-}Gal}$ for α-GAL and α-NAGAL^{EL} are zero because those enzymes show no activity towards the pNP-α-GalNAc substrate. The substrate specificity ratios for α-NAGAL and α-GAL^{SA} are similar: 57.3 ± 10.3 for α-NAGAL and 42.9 ± 9.0 for α-GAL^{SA}, showing they have comparable ability to distinguish between the two substrates.

Comparison of the enzymatic parameters of α-GAL and of α-NAGAL^{EL} (the enzyme engineered to have α-galactosidase activity) shows that the K_M values of the two enzymes are similar (6.9 and 7.6 mM respectively for the pNP-α-Gal substrate). The engineered enzyme has a turnover number k_{cat} that is approximately 1/3 that of the native α-GAL enzyme (13.7 sec^{-1} *vs*. 37.8 sec^{-1} respectively).

Comparison of the enzymatic parameters of α-NAGAL and of α-GAL^{SA} reveals that the K_M value of the engineered enzyme against the pNP-α-GalNAc substrate is 30-fold larger than that of the wild type enzyme (21.0 and 0.68 mM respectively) and 2-fold larger against the pNP-α-Gal substrate (49.1 and 27.5 mM respectively). The turnover numbers k_{cat} of α-NAGAL and α-GAL^{SA} are similar against the pNP-α-GalNAc substrate (15.1 and 21.5 sec^{-1} respectively) and differ 9-fold against the pNP-α-Gal substrate (10.7 *vs*. 1.2 sec^{-1})

Overall the kinetic parameters show that, although the engineered enzymes are not as efficient as their wild-type counterparts, they have the same ability to discriminate among different substrates as their wild-type equivalents. In particular, the α-GAL^{SA} engineered enzyme is somewhat less effective at catalyzing the turnover of substrate compared to its wild type equivalent, α-NAGAL.

Crystal structures

To examine the structural basis for the reduced catalytic efficiency of the α-GAL^{SA} enzyme, we determined four crystal structures of α-GAL^{SA} in complex with three different ligands, N-acetylgalactosamine (GalNAc), galactose, and glycerol (Table 2 and Fig. 2A-C). Superposition of α-GAL^{SA} and α-NAGAL

by their $(\beta/\alpha)_8$ barrel domains results in an RMS deviation of 0.58 Å for 290 Cα atoms in the domain. Remarkably, the superposition of the entire $(\beta/\alpha)_8$ domains shows that the GalNAc ligands and the active site residues superimpose nearly exactly (Figure 2D). Although 54% of the residues differ between α-NAGAL and α-GAL^{SA}, the ligands superimpose with an RMS deviation of 0.38 Å for the 15 atoms in the ligand.

Superposition of the $(\beta/\alpha)_8$ barrel domains of α-GAL^{SA} and α-GAL shows that the active site residues and ligands superimpose closely, except for E203 and L206 in α-GAL, which are replaced with S and A in α-GAL^{SA} (Figure 2E). The structure of α-GAL^{SA} with galactose bound shows a shift in the location of the catalytic nucleophile D170 relative to its location in other structures in the family. The D170 nucleophile shifts into the empty space produced by the reduction in size of the side chain in the E203S substitution. This shift affects the hydrogen bonding of D170 to Y134 and Y207, and likely contributes to the reduced catalytic efficiency of the α-GAL^{SA} variant protein.

The crystallographic experiments used the cryoprotectant glycerol, which appeared in the active site of α-GAL^{SA}. We determined two structures of glycerol-soaked α-GAL^{SA} in space groups $C222_1$ and $P2_12_12_1$. Because each crystal has two monomers of the protein in the asymmetric unit, we have four crystallographically-independent active site complexes with glycerol. One of the four glycerol-soaked monomers shows significant changes in the active site: the glycerol binds in a different orientation, the R227 side chain rotamer changes, and the β6-α6 loop containing the catalytic acid/base D231 shifts as well (Figure 2F). This large rearrangement in the active site is unique to α-GAL^{SA} among the glycosidase family 27 structures and may also contribute to the reduced catalytic efficiency of α-GAL^{SA}.

Discussion

The active site of human α-GAL is unable to accommodate 2-N-acetylated ligands due to steric clashes between the protein and the N-acetyl group on the ligand. Here, we have engineered α-GAL^{SA}, the first α-GAL enzyme capable of binding α-GalNAc ligands. In the reciprocal experiment, the engineered α-NAGAL^{EL} enzyme has lost all of its activity against α-GalNAc ligands and has enhanced activity against α-galactosides.

Enzyme replacement therapy

Enzyme replacement therapy can successfully treat Fabry disease. However, up to 88% of male patients develop an immune response to the injected recombinant enzyme, including both IgG- and IgE-based reactions (6,8,23). The antigenicity of the glycoproteins used in enzyme replacement therapy for Fabry disease patients might limit the effectiveness of the treatment by reducing the amount of enzyme effectively delivered to the lysosomes. We envision the α-NAGAL^{EL} molecule would have little immunogenicity in Fabry disease patients (who make typical amounts α-NAGAL glycoprotein and are thus immunologically tolerant toward α-NAGAL). Consistent with this, heterozygous female Fabry disease patients (with one wild-type copy of the GLA gene) do not make the comparable immune responses as their hemizygous male counterparts against injected enzyme during enzyme replacement therapy (24,25).

Although patients with the severe form of Fabry disease have little or no α-GAL enzyme activity, patients with the variant forms of Fabry disease can have from 5 to 35% of wild type enzyme activity (26,27). This suggests that the threshold level of α-GAL enzymatic activity necessary to prevent Fabry disease symptoms is less than 100% wild type activity. Although the enzymatic activity of the engineered proteins is lower than their wild-type equivalents, in enzyme replacement therapy, the reduced immunogenicity of the designed proteins might compensate for their reduced activity.

Sakuraba and colleagues have also tested this hypothesis by reporting a protein similar in design to α-NAGAL^{EL}, but expressed in Chinese hamster ovary cells, leading to a different glycosylation pattern (14). When injected in a mouse model of Fabry disease, the mammalian-expressed protein led to a

reduction in the amount of Gb3 in the tissues of the mouse. This further suggests that the designed enzyme might act as a useful tool for the treatment of Fabry disease.

Properties of the engineered enzymes

Western blotting with anti α-GAL and anti α-NAGAL antibodies shows that the former reacts only with α-GAL and α-GAL^{SA}, while the latter reacts only with α-NAGAL and α-NAGAL^{EL}. The sequence divergence between α-GAL and α-NAGAL is sufficient to show no immunological cross reactivity. Thus, engineering the active sites of α-GAL and α-NAGAL to have novel substrate specificities leads to new enzyme activities without altering antigenicity. This approach may be useful as a general strategy for protein-based therapeutics where reducing immunogenicity is an issue, such as Gaucher disease, where 15% of patients on enzyme replacement therapy develop IgG antibodies to the recombinant enzyme (28).

The diverse sequences in glycoside hydrolase family 27 (which includes human α-GAL and α-NAGAL) show high conservation of the active site residues, indicating strong evolutionary pressure on the active site. One modular component of ligand binding in the family is the recognition of the 2- position of the sugar ring. In this family, a single loop on the protein, the β5-α5 loop in the N-terminal domain, interacts with the substituent on the 2-position of the sugar. The similarity across the members of the family allowed us to interconvert the ligand recognition through substitution of two residues in the loop. The modularity of the loop is also seen in the structures of other members of the family, including the rice and *Hypocrea jecorina* α-GAL structures, where one turn of helix in the β5-α5 loop is replaced with a shorter loop and a longer β5 strand (12,29). In those structures, Cys and Trp residues fill the space of the E203 and L206 residue of α-GAL or the S188 and A191 residues in α-NAGAL.

The newly engineered enzymes α-GAL^{SA} and α-NAGAL^{EL} are not as catalytically efficient as their wild-type equivalents. The structures of α-GAL^{SA} suggest that there is considerably more flexibility in the active site of the α-GAL^{SA} enzyme when compared to α-NAGAL, the enzyme with an identical active site constellation.

The glycerol-soaked structures of α-GAL^{SA} provide a structural explanation for the reduced catalytic efficiency of the engineered enzyme. When the larger E203 and L206 residues of α-GAL are replaced with smaller S and A residues in α-GAL^{SA}, the active site has more open space in it. This allows the R227 side chain to move toward the space vacated by the shortening of the E203 side chain, and the β6-α6 loop containing D231 moves toward the space vacated by the shortening of the L206 side chain. The crystal structures indicate that the active site of α-GAL^{SA} is more dynamic than the active sites of the wild type enzymes α-GAL and α-NAGAL, which might explain the reduced catalytic efficiency of the designed α-GAL^{SA} enzyme. Another indication of the higher mobility of the active site of α-GAL^{SA} appears in the glycerol-soaked α-GAL^{SA} structure, which has higher atomic B-factors in the rearranged β6-α6 loop.

In this report, we describe the first instance of bidirectional interconversion of the enzymatic activities of two human lysosomal enzymes. Rational design of enzymatic function is a challenging task and generally requires large changes in the active site: for example, the classic case of conversion of trypsin activity into that of chymotrypsin required 11 substitutions in four sites on the protein (30). In general, changing substrate specificity is easier than changing the reaction mechanism of an enzyme (31). The family of lysosomal glycosidases might prove to be a fruitful target for further enzyme engineering, since many glycosidases use a similar mechanism with an arrangement of two carboxylates located on opposite sides of the glycosidic linkage to be cleaved.

In conclusion, we have shown the viability of a rational design approach to engineering new functionality into human lysosomal enzymes. This approach allows for encoding new enzymatic functions into existing protein scaffolds. By reusing existing proteins in new ways, our approach avoids the immunogenicity problems that are frequently seen in enzyme replacement therapies. This

approach might also be used for a wide range of protein-based therapeutics when immunogenicity problems exist.

References

1. Desnick, R. J., Ioannou, Y. A., and Eng, C. M. (2001) α-Galactosidase A Deficiency: Fabry Disease. in *The Metabolic and Molecular Bases of Inherited Disease* (Scriver, C. R., Beaudet, A. L., Sly, W. S., and Valle, D. eds.), 8th Ed., McGraw-Hill, New York. pp 3733-3774
2. Spada, M., Pagliardini, S., Yasuda, M., Tukel, T., Thiagarajan, G., Sakuraba, H., Ponzone, A., and Desnick, R. J. (2006) *Am J Hum Genet* **79**, 31-40
3. Desnick, R. J., and Schindler, D. (2001) α-N-Acetylgalactosaminidase Deficiency: Schindler Disease. in *The Metabolic and Molecular Bases of Inherited Disease* (Scriver, C. R., Beaudet, A. L., Sly, W. S., and Valle, D. eds.), 8th Ed., McGraw-Hill, New York. pp 3483-3505
4. Wang, A. M., Bishop, D. F., and Desnick, R. J. (1990) *J. Biol. Chem.* **265**, 21859-21866
5. Cantarel, B. L., Coutinho, P. M., Rancurel, C., Bernard, T., Lombard, V., and Henrissat, B. (2009) *Nucleic Acids Res* **37**, D233-238
6. Eng, C. M., Guffon, N., Wilcox, W. R., Germain, D. P., Lee, P., Waldek, S., Caplan, L., Linthorst, G. E., and Desnick, R. J. (2001) *N. Engl. J. Med.* **345**, 9-16
7. Schiffmann, R., Kopp, J. B., Austin, H. A., 3rd, Sabnis, S., Moore, D. F., Weibel, T., Balow, J. E., and Brady, R. O. (2001) *JAMA* **285**, 2743-2749
8. Schiffmann, R., Ries, M., Timmons, M., Flaherty, J. T., and Brady, R. O. (2006) *Nephrol Dial Transplant* **21**, 345-354
9. Garman, S. C., and Garboczi, D. N. (2004) *J Mol Biol* **337**, 319-335
10. Clark, N. E., and Garman, S. C. (2009) *J Mol Biol* **393**, 435-447
11. Garman, S. C., Hannick, L., Zhu, A., and Garboczi, D. N. (2002) *Structure* **10**, 425-434
12. Fujimoto, Z., Kaneko, S., Momma, M., Kobayashi, H., and Mizuno, H. (2003) *J Biol Chem* **278**, 20313-20318
13. Garman, S. C. (2006) *Biocat and Biotrans* **24**, 129-136
14. Tajima, Y., Kawashima, I., Tsukimura, T., Sugawara, K., Kuroda, M., Suzuki, T., Togawa, T., Chiba, Y., Jigami, Y., Ohno, K., Fukushige, T., Kanekura, T., Itoh, K., Ohashi, T., and Sakuraba, H. (2009) *Am J Hum Genet* **85**, 569-580
15. Guce, A. I., Clark, N. E., Salgado, E. N., Ivanen, D. R., Kulminskaya, A. A., Brumer, H., 3rd, and Garman, S. C. (2010) *J Biol Chem* **285**, 3625-3632
16. Otwinowski, Z., and Minor, W. (1997) Processing of X-ray Diffraction Data Collected in Oscillation Mode. in *Methods in Enzymology : Macromolecular Crystallography, part A* (C.W. Carter, J. R. M. S., Eds ed.), Academic Press. pp 307-326
17. Collaborative Computational Project, N. (1994) *Acta Crystallogr.* **D50**, 760-763
18. Jones, T. A., Zou, J. Y., Cowan, S. W., and Kjeldgaard, M. (1991) *Acta Crystallogr. A* **47**, 110-119
19. Laskowski, R. A., Macarthur, M. W., Moss, D. S., and Thornton, J. M. (1993) *J. Appl. Crystallog.* **26**, 283-291
20. Kleywegt, G. J., and Read, R. J. (1997) *Structure* **5**, 1557-1569
21. Kraulis, P. J. (1991) *J. Appl. Crystallogr.* **24**, 946-950
22. Fenn, T. D., Ringe, D., and Petsko, G. A. (2003) *J. Appl. Cryst.* **36**, 944-947
23. Bodensteiner, D., Scott, C. R., Sims, K. B., Shepherd, G. M., Cintron, R. D., and Germain, D. P. (2008) *Genet Med* **10**, 353-358
24. Vedder, A. C., Breunig, F., Donker-Koopman, W. E., Mills, K., Young, E., Winchester, B., Ten Berge, I. J., Groener, J. E., Aerts, J. M., Wanner, C., and Hollak, C. E. (2008) *Mol Genet Metab* **94**, 319-325
25. Benichou, B., Goyal, S., Sung, C., Norfleet, A. M., and O'Brien, F. (2009) *Mol Genet Metab* **96**, 4-12

26. Mayes, J. S., Scheerer, J. B., Sifers, R. N., and Donaldson, M. L. (1981) *Clin Chim Acta* **112**, 247-251
27. Ries, M., Gupta, S., Moore, D. F., Sachdev, V., Quirk, J. M., Murray, G. J., Rosing, D. R., Robinson, C., Schaefer, E., Gal, A., Dambrosia, J. M., Garman, S. C., Brady, R. O., and Schiffmann, R. (2005) *Pediatrics* **115**, 344-355
28. Starzyk, K., Richards, S., Yee, J., Smith, S. E., and Kingma, W. (2007) *Mol Genet Metab* **90**, 157-163
29. Golubev, A. M., Nagem, R. A., Brandao Neto, J. R., Neustroev, K. N., Eneyskaya, E. V., Kulminskaya, A. A., Shabalin, K. A., Savel'ev, A. N., and Polikarpov, I. (2004) *J Mol Biol* **339**, 413-422
30. Perona, J. J., Hedstrom, L., Rutter, W. J., and Fletterick, R. J. (1995) *Biochemistry* **34**, 1489-1499
31. Toscano, M. D., Woycechowsky, K. J., and Hilvert, D. (2007) *Angew Chem Int Ed Engl* **46**, 3212-3236

Acknowledgements

This work was funded by NIH grant R01 DK76877 to S.C.G. and by NSF Integrative Graduate Education and Research Traineeship 0654128 to N.E.C. We gratefully acknowledge Jean Jankonic, Marc Allaire, and Vivian Stojanoff at the National Synchrotron Light Source X6A beam line, funded by the National Institute of General Medical Sciences, National Institute of Health under agreement GM-0080. We thank Igor Kourinov and the staff of the Advanced Photon Source Northeastern Collaborative Access Team beamlines, which are supported by award RR-15301 from the National Center for Research Resources at the National Institutes of Health. Use of the Advanced Photon Source was supported by the U.S. Department of Energy, Office of Basic Energy Sciences, under Contract No. DE-AC02-06CH11357.

Figure Legends

Figure 1: α-GAL and α-NAGAL structural and biochemical analyses

A: Sequence alignment of the α-GAL and α-NAGAL proteins. Active site residues are red, and identities have yellow backgrounds. The two active site residues that differ are boxed. B and C: Ribbon diagrams of α-GAL (green) and α-NAGAL (cyan) with attached carbohydrates. Insets show the active sites of α-GAL and α-NAGAL with their catalytic products α-galactose and α-GalNAc respectively (white). 11 of the 13 active site residues are conserved between the enzymes, although the overall sequence identity is 46%. The two residues that differ (E203 and L206 in α-GAL; S188 and A191 in α-NAGAL) select for the substituent on the 2- position of the ligand. D: The four purified proteins are shown on a Coomassie-stained SDS gel. α-GAL and α-GAL^{SA} (with 3 N-linked glycosylation sites each) run smaller on the SDS gel than α-NAGAL and α-$NAGAL^{EL}$ (with five N-linked glycosylation sites each). E: Western Blots of the four proteins, detected with polyclonal anti-α-GAL (top) and polyclonal anti-α-NAGAL antibodies (bottom). The variant proteins retain the antigenicity of the original proteins.

Figure 2: α-GAL^{SA} crystal structures

A, B, and C: σ_A-weighted $2F_o$-F_c total omit electron density maps of α-GAL^{SA} calculated in SFCHECK (17). A: GalNAc-soaked crystal contoured at 2.0σ. B: Galactose-soaked crystal contoured at 1.8σ. C: Glycerol-soaked crystal soaked at 1.0σ. Maps have a cover radius drawn around ligands and/or waters in the active site. Active site residues are labeled in (A). D: A superposition of crystal structures of the active sites of α-GAL^{SA} and α-NAGAL, each with α-GalNAc bound in the active site. When the structures are superimposed by their $(\beta/\alpha)_8$ barrels, the ligands superimpose nearly exactly. E: A superposition of crystal structures of the active sites of α-GAL^{SA} and α-GAL, each with α-galactose bound in the active site. F: A superposition of the four monomers of glycerol-soaked α-GAL^{SA}, with glycerol bound in the active site. In one of the four structures (green), the glycerol binds in a vertical orientation, and shows differences in R227 and the loop containing D231 (arrows).

Tables

Table 1: Enzymatic parameters

Substrate:	**pNP-α-Gal**			**pNP-α-GalNAc**		
Enzyme	**K_M (mM)**	**k_{cat} (sec^{-1})**	**k_{cat} / K_M (mM^{-1} sec^{-1})**	**K_M (mM)**	**k_{cat} (sec^{-1})**	**k_{cat} / K_M (mM^{-1} sec^{-1})**
α-GAL	6.88 ± 0.07	37.8 ± 0.2	5.49 ± 0.06		No activity detected *	
α-NAGAL^{EL}	7.58 ± 0.07	13.7 ± 0.1	1.81 ± 0.02		No activity detected *	
α-NAGAL	27.5 ± 4.7	10.7 ± 0.9	0.39 ± 0.07	0.68 ± 0.01	15.1 ± 0.1	22.4 ± 0.1
α-GAL^{SA}	49.1 ± 7.2	1.20 ± 0.14	0.024 ± 0.005	21.0 ± 0.8	21.5 ± 0.7	1.03 ± 0.03

* $k_{cat} < 0.01$ sec^{-1}

Table 2: α-GAL^{SA} Data Collection and Refinement Statistics

Ligand:	GalNAc	Galactose	Glycerol	Glycerol
PDB ID:	3LX9	3LXA	3LXB	3LXC
Data Collection:				
Beamline	APS 24-ID-C	NSLS X6A	NSLS X6A	APS 24-ID-C
Wavelength (Å)	1.07188	0.98010	0.98010	1.07188
Space group	$C222_1$	$P2_12_12_1$	$P2_12_12_1$	$C222_1$
Resolution (Å) (last shell)	50-2.05 (2.09-2.05)	50-3.0 (3.11-3.0)	50-2.85 (2.90-2.85)	50-2.35 (2.39-2.35)
Cell parameters *a*, *b*, *c* (Å)	89.95, 139.49, 182.58	59.50, 105.85, 181.85	59.57, 106.92, 181.51	89.75, 139.77, 182.45
No. of observations	481,042	172,299	136,330	193,566
No. of unique observations (last shell)	72,009 (3,354)	23,638 (2,309)	27,897 (1,334)	47,535 (2,335)
Multiplicity (last shell)	6.7 (3.6)	7.3 (7.2)	4.9 (4.9)	4.1 (4.0)
Completeness (%) (last shell)	99.4 (93.3)	100.0 (99.9)	99.3 (99.9)	98.6 (98.7)
R_{sym} (last shell)	0.120 (0.701)	0.271 (0.851)	0.177 (0.616)	0.153 (0.862)
I/σ_I (last shell)	18.6 (1.6)	7.6 (1.8)	9.1 (2.2)	12.3 (2.0)
Refinement:				
R_{work}/R_{free} , %	17.62/21.82	21.45/24.39	22.50/26.38	18.35/23.68
No. of atoms	7057	6557	6657	7032
Protein	6241	6303	6320	6241
Carbohydrate	257	218	170	227
Water	559	36	131	552
Other	0	0	36	12
Average B, Å^2	37.5	34.5	32.5	45.3
Protein Average B, Å^2	36.3	33.9	31.8	44.4
Ramachandran Plot:				
Favored (%)	91.4	89.5	89.5	89.7
Allowed (%)	8.0	9.6	9.6	9.5
Generous (%)	0.3	0.6	0.9	0.7
Forbidden (%)	0.3	0.3	0.0	0.1
RMS deviations:				
Bonds (Å)	0.0053	0.0150	0.0088	0.0081
Angles (°)	1.056	1.502	1.222	1.172

$R_{sym}=\Sigma_h\Sigma_i|I_{h,i}-\langle I_h\rangle|/\Sigma_h\Sigma_i|I_{h,i}|$, where $I_{h,i}$ is the i^{th} intensity measurement of reflection h and $\langle I_h\rangle$ is the average intensity of that reflection.

R_{work} , $R_{free}=\Sigma_h|F_P-F_C|/\Sigma_h|F_P|$, where F_C is the calculated and F_P is the observed structure factor amplitude of reflection h for the working or free set, respectively.

Ramachandran statistics were calculated in PROCHECK.

Figure 1

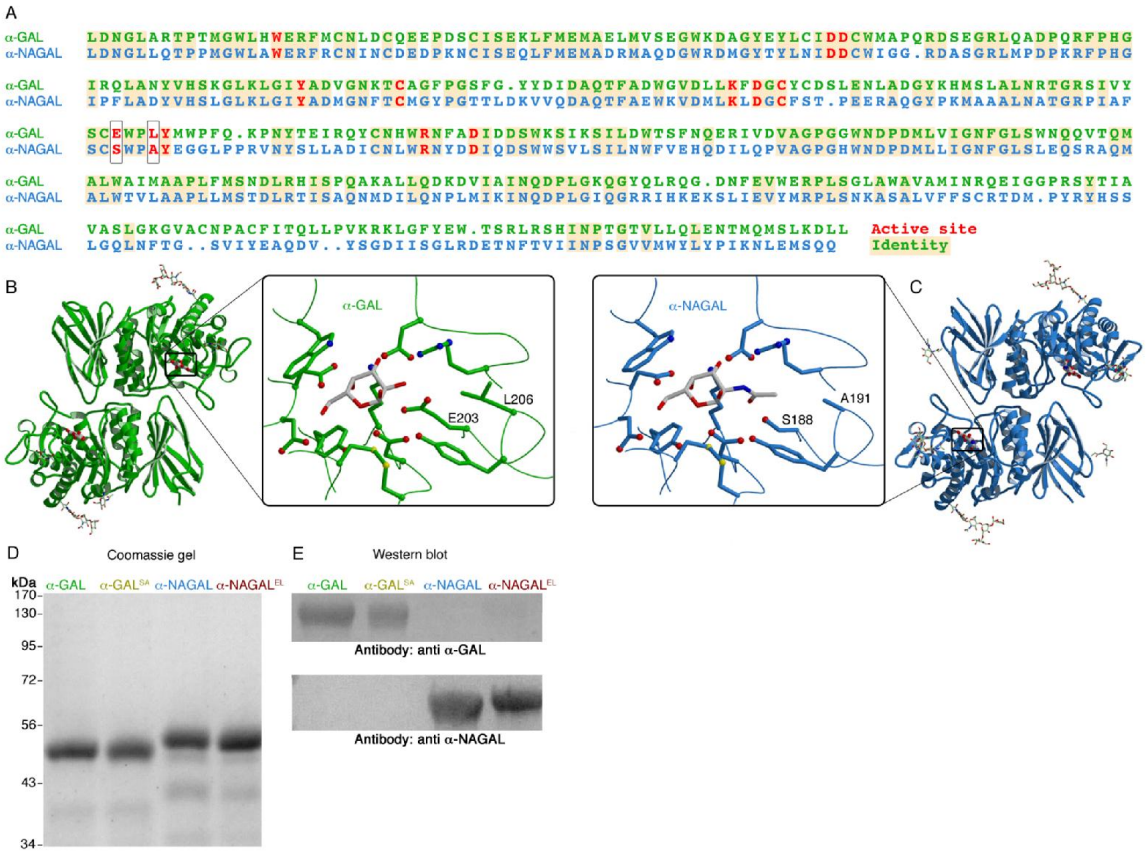
A
α-GAL LDNGLARTPTMGWLHWERFMCNLDCQEEPDSCISEKLFMEMAELMVSEGWKDAGYEYLCIDDCWMAPQRDSEGRLQADPQRFPHG
α-NAGAL LDNGLLQTPPMGWLAWERFRCNINCDEDPKNCISEQLFMEMADRMAQDGWRDMGYTYLNIDDCWIGG.RDASGRLMPDPKRFPHG
α-GAL IRQLANYVHSKGLKLGIYADVGNKTCAGFPGSFG.YYDIDAQTFADWGVDLLKFDGCYCDSLENLADGYKHMSLALNRTGRSIVY
α-NAGAL IPFLADYVHSLGLKLGIYADMGNFTCMGYPGTTLDKVVQDAQTFAEWKVDMLKLDGCFST.PEERAQGYPKMAAALNATGRPIAF
α-GAL SCEWPLYMWPFQ.KPNYTEIRQYCNHWRNFADIDDSWKSIKSILDWTSFNQERIVDVAGPGGWNDPDMLVIGNFGLSWNQQVTQM
α-NAGAL SCSWPAYEGGLPPRVNYSLLADICNLWRNYDDIQDSWWSVLSILNWFVEHQDILQPVAGPGHWNDPDMLLIGNFGLSLEQSRAQM
α-GAL ALWAIMAAPLFMSNDLRHISPQAKALLQDKDVIAINQDPLGKQGYQLRQG.DNFEVWERPLSGLAWAVAMINRQEIGGPRSYTIA
α-NAGAL ALWTVLAAPLLMSTDLRTISAQNMDILQNPLMIKINQDPLGIQGRRIHKEKSLIEVYMRPLSNKASALVFFSCRTDM.PYRYHSS
α-GAL VASLGKGVACNPACFITQLLPVKRKLGFYEW.TSRLRSHINPTGTVLLQLENTMQMSLKDLL
α-NAGAL LGQLNFTG..SVIYEAQDV..YSGDIISGLRDETNFTVIINPSGVVMWYLYPIKNLEMSQQ
Active site
Identity
B
α-GAL
L206
E203
α-NAGAL
A191
S188
C
D
Coomassie gel
kDa
α-GAL
α-GAL^SA
α-NAGAL
α-NAGAL^EL
170
130
95
72
56
43
34
E
Western blot
α-GAL
α-GAL^SA
α-NAGAL
α-NAGAL^EL
Antibody: anti α-GAL
Antibody: anti α-NAGAL

Figure 2

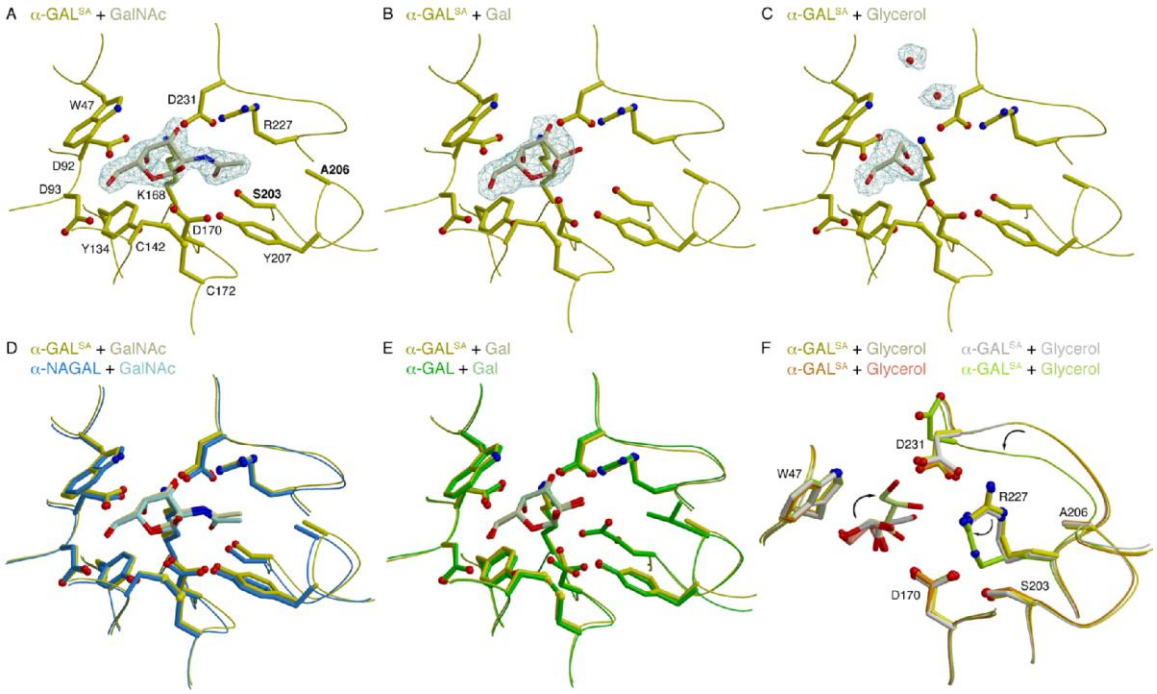
A α-GALSA + GalNAc
W47
D231
R227
D92
A206
D93
K168
S203
D170
Y134
C142
Y207
C172
B α-GALSA + Gal
C α-GALSA + Glycerol
D α-GALSA + GalNAc
α-NAGAL + GalNAc
E α-GALSA + Gal
α-GAL + Gal
F α-GALSA + Glycerol
α-GALSA + Glycerol
α-GALSA + Glycerol
α-GALSA + Glycerol
D231
W47
R227
A206
D170
S203

BIBLIOGRAPHY

1) Desnick, R. J., Ioannou, Y. A., Eng, C. M. "α -Galactosidase A Deficiency: Fabry Disease, The Metabolic and Molecular Bases of Inherited Disease." Sciver, C.R., et al., Editors. 2001, McGraw-Hill: New York, p. 3733-3774.

2) Brady, R. O. (1967) "Enzymatic Deficiencies in Fabry Disease. Ceramidetrihexosidase Deficiency." *N. Engl. J. Med*., **276**, 1163-167.

3) Garman, S.C., Garboczi, D. N. (2004) "The Molecular Defect Leading to Fabry Disease: Structure of Human α-Galactosidase." *J. Mol. Biol*., **337**, 319-335.

4) Elstein, D., Beck, M., Altrarescu, G. eds. "Fabry Disease." New York: Springer-Verlag LCC, 2010.

5) MacDermot, K.D., Holmes, A., Miners, A.H. (2009) "Anderson-Fabry Disease: Clinical Manifestations and Impact of Disease in Cohort of 60 Obligate Carrier Females." *J. Med. Genet*., **38**, 769-807.

6) Breunig, F., Wanner, C. (2003) "Enzyme Replacement Therapy for Fabry Disease: Proving the Clinical Benefit." *Nephrology Dialysis Transplantation*, **18**, 7-9.

7) Eng, C. M., Guffon, N., Wilcox, W. R., Germain, D. P., Lee, P., Waldek, S., Caplan, L., Linthorst, G. E., Desnick, R. J. (2001) "Safety and Efficacy of Recombinant Human α-Galactosidase A Replacement Therapy in Fabry Disease." *N. Engl. J. Med*., **345**, 9–16.

8) Schiffmann, R., Ries, M., Timmons, M., Flaherty, J. T., Brady, R. O. (2006) "Long-Term Therapy with Agalsidase Alfa for Fabry Disease: Safety and Effects on Renal Function in a Home Infusion Setting." *Nephrol. Dial. Transplant*., **21**, 345-354.

9) Genzyme Corporation. "Fabrazyme Agalsidase Beta; Highlights of Prescribing Information." Fabrazyme. Dec. 2008. Web. <http://www.fabrazyme.com>.

10) Shire Human Genetic Therapies. "Replagal Summary of Product Characteristics." Replagal ® (Agalsidase Alfa). 2009. Web. <http://www.replagal.com>.

11) Vedder, A. C., Breunig, F., Donker-Koopman, W. E., Mills, K., Young, E., Winchester, B., Ten Berge, I.J.M., Groener, J.E.M., Aerts, J.M.F.G., Wanner, C., Hollak, C. E.M. (2008) "Treatment of Fabry Disease with Different Dosing Regimens of Agalsidase: Effects on Antibody Formation and GL-3." *Molecular Genetics and Metabolism*, **94**, 319-25.

12) Hollak, C.E.M., Linthorst, G.E. (2009) "Immune Responces to Enzyme Replacement Therapy in Fabry Disease: Impact on Clinical Outcome." *Molecular Genetics and Metabolism*, **96**, 1-3.

13) Lee, K., Jin, X., Zhang, K., Copertino, L., Andrews, L., Baker-Malcolm, J., Geagan, L., Qiu, H., Seiger, K., Barngrover, D., McPherson, J., Edmunds, T. (2003) "A Biochemical and Pharmacological Comparison of Enzyme Replacement Therapies for the Glycolipid Storage Disorder Fabry Disease." *Glycobiology*, **13**, 305-13.

14) Frustaci, A., Chimenti, C., Ricci, R., Natale, N., Russo, M.A., Pieroni, M., Eng, C. M., Desnick, R. J. (2001) "Improvement in Cardiac Function in the Cardiac Variant of Fabry's Disease with Galactose-Infusion Therapy." *N. Engl. J. Med*., **345**, 25-32.

15) Garman, S. C., Hannick, L., Zhu, A., Garboczi, D. N. (2002) "The 1.9 Å Structure of α-N-acetylgalactosaminidase: Molecular Basis of Glycosidase Deficiency Diseases." *Structure*, **10**, 425–434.

16) Clark, N. E., Garman, S. C., (2009) "The 1.9 Å Structure of Human α -N-acetylgalactosaminidase: The Molecular Basis of Schindler and Kanzaki Diseases." *J. Mol. Biol.*, **398**, 435-47.

17) Fan, Jian-Qiang. (2003) "A Contradictory Treatment for Lysosomal Storage Disorders: Inhibitors Enhance Mutant Enzyme Activity." *Trends in Pharmacological Sciences*, **24**, 355-60.

18) Garman, S. C., (2006) "Structural Studies on α-GAL and α-NAGAL: The Atomic Basis of Fabry and Schindler Diseases." *Biocatalysis and Biotransformation*, **24**, 129-136.

19) O'Reilly, D. R., Miller, L. K., Luckow, V. A. "Baculovirus Expression Vectors: a Laboratory Manual*."* New York: Oxford UP, 1994.

20) Lodish, H., Baltimore, D., Berk, A., Matsudaira, P., Zipursky, L. S., Darnell, J. "Molecular Cell Biology." 3rd ed. New York: Scientific American, 1998.

21) Guce, A.I., Clark, N.E., Salgado, E.N., Ivanen, D.R., Kulminskaya, A.A., Brumer, H. 3rd., Garman, S.C. (2009) "Catalytic Mechanism of Human α-Galactosidase." *J. Biol. Chem*., **285**, 3625-32.

22) Tajima, Y., Kawashima, I., Tsukimura, T., Sugawara, K., Kuroda, M., Suzuki, T., Togawa, T., Chiba, Y., Jigami, Y., Ohno, K., Fukushige, T., Kanekura, T., Itoh, K., Ohashi, T., and Sakuraba, H. (2009) "Use of a Modified α-N-acetylgalactosaminidase in the Development of Enzyme Replacement Therapy for Fabry Disease." *Am. J. Hum. Genet.*, **85**, 569-580.

23) Perona, J. J., Hedstrom, L., Rutter, W. J., and Fletterick, R. J. (1995) "Structural Origins of Substrate Discrimination in Trypsin and Chymotripsin." *Biochemistry*, **34**, 1489-1499.

24) Collaborative Computational Project, N. (1994) *Acta Crystallogr.* **D50**, 760-763

25) Jones, T. A., Zou, J. Y., Cowan, S. W., and Kjeldgaard, M. (1991) "Improved Methods for Building Protein Models in Electron Density Maps and the Location of Errors in these Models." *Acta Crystallogr. A* **47**, 110-119

26) Laskowski, R. A., Macarthur, M. W., Moss, D. S., and Thornton, J. M. (1993) *J. Appl. Crystallog.* **26**, 283-291

27) Kleywegt, G. J., Read, R. J. (1997) "Not your Average Density." *Structure.* **5,** 1557-1569